

Original Research

P53-independent partial restoration of the p53 pathway in tumors with mutated p53 through ATF4 transcriptional modulation by ERK1/2 and CDK9



Xiaobing Tian^{1,2,3,5,6}; Nagib Ahsan^{2,4,5}; Amriti Lulla⁶; Avital Lev⁶; Philip Abbosh⁶; David T. Dicker^{1,2,3,5,6}; Shengliang Zhang^{1,2,3,5,6}; Wafik S. El-Deiry^{1,2,3,5,6,7}

¹ Laboratory of Translational Oncology and Experimental Cancer Therapeutics, The Warren Alpert Medical School, Brown University, Providence, RI, USA

² The Joint Program in Cancer Biology, Brown University and Lifespan Health System, Providence, RI, USA

³ Department of Pathology and Laboratory Medicine, Brown University Alpert Medical School, Providence, RI, USA

⁴ COBRE Center for Cancer Research Development, Proteomics Core Facility, Rhode Island Hospital, Providence, RI, USA

⁵ Division of Biology and Medicine, Brown University, Providence, RI, USA

⁶ Molecular Therapeutics Program, Fox Chase Cancer Center, Philadelphia, PA, USA

⁷ Hematology-Oncology Division, Department of Medicine, Rhode Island Hospital and Brown University, Providence, RI, USA

Abstract

A long-term goal in the cancer-field has been to develop strategies for treating p53-mutated tumors. A novel small-molecule, PG3-Oc, restores p53 pathway-signaling in tumor cells with mutant-p53, independently of p53/p73. PG3-Oc partially upregulates the p53-transcriptome (13.7% of public p53 target-gene dataset; 15.2% of in-house dataset) and p53-proteome (18%, HT29; 16%, HCT116-p53^{-/-}). Bioinformatic analysis indicates critical p53-effectors of growth-arrest (p21), apoptosis (PUMA, DR5, Noxa), autophagy (DRAM1), and metastasis-suppression (NDRG1) are induced by PG3-Oc. ERK1/2- and CDK9-kinases are required to upregulate ATF4 by PG3-Oc which restores p53 transcriptomic-targets in cells without functional-p53. PG3-Oc represses MYC (ATF4-independent), and upregulates PUMA (ATF4-dependent) in mediating cell death. With largely nonoverlapping transcriptomes, induced-ATF4 restores p53 transcriptomic targets in drug-treated cells including functionally important mediators such as PUMA and DR5. Our results demonstrate novel p53-independent drug-induced molecular reprogramming involving ERK1/2, CDK9, and ATF4 to restore upregulation of p53 effector genes required for cell death and tumor suppression.

Neoplasia (2021) 23, 304–325

Keywords: Cancer therapy, Mutant p53, p53 pathway restoration, PG3-Oc, ERK1/2, CDK9, MYC, PUMA, ATF4, DR5

Introduction

The p53 transcription factor is activated by various cellular stresses such as DNA damage, oncogene activation, nutrient depletion, oxidative stress and endoplasmic reticulum (ER) stress [1–3]. The tumor suppressor p53 regulates complicated transcription programs that respond to particular stress signals in maintaining homeostasis and guarding the genome. There are 3 main outcomes after the activation of p53: cell-cycle arrest, senescence, and apoptosis. Cell-cycle arrest allows cell repair and recovery from the stress, so that cell survival occurs. Senescence and apoptosis are terminal and irreversible. It has been proposed that the nature of the stress signal, the nature of the compound, the duration of the stress signal and the cell type determine the transcriptional program of p53, and the phenotypic outcome in the stressed cell [4,5]. Thus, when p53 is activated, a specific set of p53

Abbreviations: DMSO, dimethyl sulfoxide; ER, endoplasmic reticulum; GRO, global run-on; IPA, ingenuity pathway analysis.

* Corresponding author.

E-mail address: wafik@brown.edu (W.S. El-Deiry).

Received 1 December 2020; received in revised form 20 January 2021; accepted 25 January 2021

© 2021 The Authors. Published by Elsevier Inc. This is an open access article under the CC BY-NC-ND license (<http://creativecommons.org/licenses/by-nc-nd/4.0/>) (<http://doi.org/10.1016/j.neo.2021.01.004>)

target genes is regulated, instead of all of the p53 target genes, with tissue specificity [6]. In addition, specific gene sets of p53-activated changes occur over time in cells following a stressor. For example, HCT116 and HCT116 p53^{-/-} cells treated with the MDM2 inhibitor nutlin-3 for 1 h, followed by global run-on sequencing (GRO-Seq), identified 198 possible direct targets of p53 [7]. Both CHIP-seq and RNA-seq analysis identified 432 direct p53 target genes in mouse MEF cells treated with the DNA damage-inducing drug doxorubicin [8]. Menendez et al. employed CHIP-seq and microarray analysis and identified 205 p53 target genes in U2OS cells. The authors reported that U2OS cells had strikingly different p53-binding patterns and transcriptional responses following exposure to the DNA-damaging agent doxorubicin vs nutlin-3 for 24 h, with nutlin-3 considered a nongenotoxic activator of p53. Genome-wide analysis of the ChIP-seq identified 3087 p53-binding sites after doxorubicin treatment and nearly 6-fold more sites (18,159) in cells treated with Nutlin-3 [9]. Meta-analysis of 4 publications (using Chip-seq assays) indicated that p53 may directly activate >1200 genes. However, only 26 of these genes were commonly activated in all 4 studies [7]. This lack of overlap is possibly due to methodological differences and cell type-specific differences [7]. Fischer identified 346 possible direct p53 target genes through searching the literature and performing meta-analysis of data from 319 studies [10]. Because this p53 target gene database is not generated from a specific drug in a specific cell line, we selected Fischer's p53 target genes as a database for evaluating the effectiveness of p53 pathway restoration by a candidate therapeutic compound. We also developed an in-house reference p53 target gene data set by RNA-Seq and p53-dependent protein data set by proteomic analysis, using HCT116 and HCT116 p53^{-/-} cell lines treated with the known p53 activator 5-Fluorouracil (5-FU) as a positive control. p53 is inactivated in almost all human cancers, either by mutation, deletion, MDM2 overexpression, or inactivation by viral proteins [1,11]. Over 50% of human cancers harbor cancer-promoting mutations in p53 [11]. p53 mutations not only abrogate its tumor-suppressor function, but also confer gain-of-function properties that contribute to tumorigenesis, proliferation, genomic instability, metabolic remodeling, invasion, metastasis, resistance to apoptosis, and cancer therapy resistance [11,12]. Hence, restoration of the p53 pathway represents an important strategy for achieving anticancer therapy in mutant p53-bearing tumors. Restoring p53 function has been tried using different approaches, which include restoration of wild-type p53 function through a small molecule that binds to mutant p53 [2,13], compound-induced degradation of mutant p53 [14,15], disruption of protein-protein interaction between mutant p53 and other transcription factors [16]. Strategies employing genome-wide restoration of the p53 pathway by small molecules via p53-independent mechanisms are considered promising, and may involve the p53 homolog p73 [15,17].

About 50% of cancer cells lack wild-type p53 due to mutation or deletion of the TP53 gene, we hypothesized that other transcription factors may compensate for p53 loss and play an important role in coping with extrinsic and intrinsic stresses, and regulate cell fate, such as survival, senescence, and apoptosis. Moreover, such factors may be possible to modulate with candidate anticancer therapeutics. Like p53, ATF4 (activating transcription factor 4), plays an important role in communicating pro-survival and pro-apoptotic signals. The ER stress kinase PERK (PKR-like ER kinase) senses various stresses and catalyzes the phosphorylation of the α -subunit of eIF2 α . Phosphorylation of eIF2 α at serine 51 attenuates global protein synthesis temporarily while selectively enhancing translation of ATF4 mRNA. Once activated, ATF4 regulates a transcriptional program involved in cell survival (antioxidant response, amino acid biosynthesis, and autophagy), senescence and apoptosis. The final outcome of ATF4 activation is dependent on the cell type, nature of stressors and duration of the stresses [18–21].

Prodigiosin is a member of a family of naturally occurring red pigments produced by microorganisms including *Streptomyces* and *Serratia* [22]. Most of the members of this family contain a common 4-

methoxy-pyrrolylpyromethene pharmacophore (Fig. 1A, red highlight). Our laboratory reported that prodigiosin shows potent anti-cancer activity against human tumors with mutated p53 through restoring the p53 pathway, in part, via p73 [17,23]. Based on the structure of the pharmacophore of the prodigiosin family, we synthesized drug analogs, including a novel compound PG3-Oc whose synthesis is described in an issued composition of matter patent [24]. We report the effects on cell signaling and anti-cancer activity of PG3-Oc. Importantly, we use PG3-Oc as a chemical probe of the cell signaling mechanisms that underlie p53 pathway restoration in a p53-independent manner. PG3-Oc induces noncanonical ER stress and partially restores the p53 pathway globally through transcription factor ATF4 leading to induction of pro-apoptotic gene targets. Insights into an ERK1/2- and CDK9-dependent ATF4-activation by PG3-Oc leading to cell death and antitumor efficacy through PUMA and DR5 are provided. Our results shed light upon the mechanisms used by a novel compound to induce p53-independent p53 pathway restoration in tumors with mutated p53, and demonstrate feasibility of the approach to partially restore the p53 transcriptome globally to achieve tumor suppression.

Materials and Methods

Cell lines and reagents

P53-mutant cell lines: HT29 (R273H), SW480 (R273H/P309S), DLD-1 (S241F), H1975 (R273H), MDA-MD-231 (R280K), U251 (R273H), FaDu (R248L), CAL-27 (H193L), PANC-1 (R273H), Aspc-1 (frameshift mutation), P53 wild-type cell lines: HCT116, and CCD 841 Con; P53-null cell line: HCT116 p53^{-/-}. H1975 and CCD 841 Con cells were purchased from ATCC. HT29, SW480, DLD-1, HCT116, FaDu, CAL-27, MDA-MD-231, PANC-1 and Aspc-1 and Jurkat cell lines were purchased from Fox Chase Cancer Center cell culture facility. HCT116 p53^{-/-} cell lines were from the Vogelstein laboratory at Johns Hopkins. Cells were verified to be MYCoplasm-free at multiple times throughout the study. We routinely checked for MYCoplasm and all cell lines underwent STR authentication. Chemicals: Caspase 8 inhibitor Z-IETD-fmk (BD Bioscience), LDC000067, NVP-2, and thapsigargin (Tocris Bioscience), MG-132, 5-FU, trametinib, PLX-4720, Z-VAD-fmk, GSK2606414, SCH772984, regorafenib, SB216763, and SP600125 (Selleck chemicals).

Western blotting

After treatment, protein lysates were collected for Western blot analysis. A total of 15 μ g of protein was used for SDS-PAGE. After primary and secondary antibody incubations, the signal was detected by a chemiluminescence detection kit, imaged by Syngene (Imgen Technologies). Antibodies for PUMA (for IHC), NAG-1 (GDF15), P53 were from Santa Cruz Biotechnology; for caspase 8, cleaved caspase 8, caspase 9, caspase 3, cleavage PARP, eIF2 α , p-eIF2 α (Ser51), CHOP, ATF4, DR5, FOXO3a, p-FOXO3a (Ser253), NF- κ B p65, p-NF- κ B p65 (Ser536), c-Jun, p-c-Jun (Ser63), JNK, p-JNK (Thr183/Tyr185), PUMA (for WB), MYC, phospho-S62-cMYC, NDRG1, Phospho-CDK9 (Thr86), CDK9, Rpb1 NTD (RNA PII subunit B1), phospho-(Ser2) Rpb1 CTD (RNA PII subunit B1), RSK, and phospho-p90RSK(Ser380) were from Cell Signaling Technology. Noxa and p21 were from Calbiochem. p73 was from Bethyl laboratories Inc., Ran was from BD Biosciences. β -actin was from Sigma.

Cell viability assay

Cells were seeded in 96-well plates (6×10^3 cells/well). Cells were treated with different concentrations of compounds or dimethyl sulfoxide (DMSO) as a control for 72 h. The cell viability was assessed by CellTiterGlo

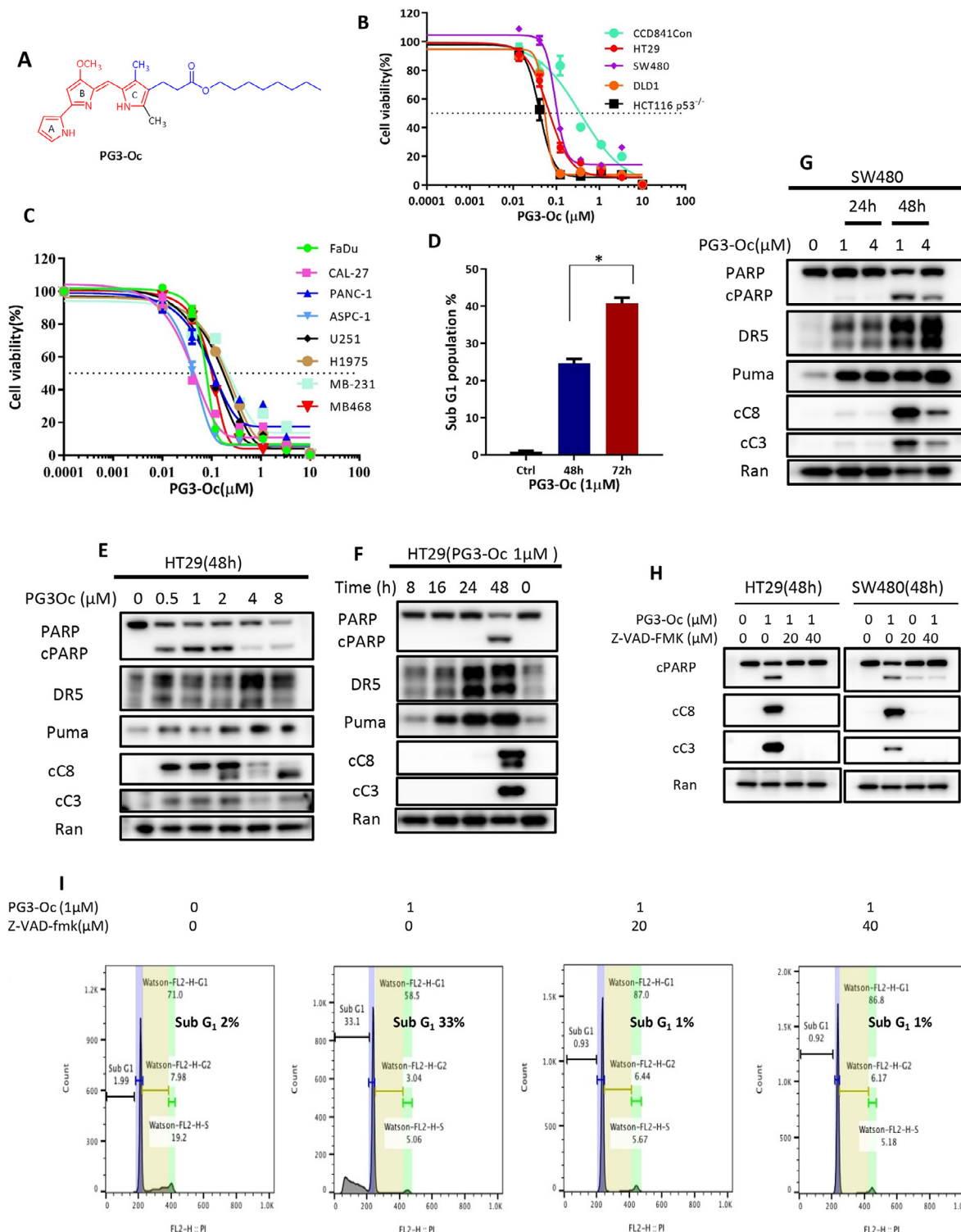


Fig. 1. PG3-Oc inhibits cell proliferation and induces apoptosis in mutant p53-expressing cancer cell lines. (A) Structure of PG3-Oc. (B) and (C) Cell viability assay, dose response curves and IC₅₀ value measurement of PG3-Oc in a panel of cancer cell lines. Cells were treated with different concentrations of PG3-Oc (Oc), or DMSO for 72 h. Luciferase activity was imaged by the IVIS Imaging System after treatment. Cell viability data were normalized to those of DMSO treatment control in each cell line and data analyses were performed using PRISM4 software. IC₅₀ data are expressed as the mean \pm SD (normal; n = 3). (D) Cell-cycle profiles after PG3-Oc treatment and apoptosis were analyzed by nuclear PI-staining using flow cytometry. HT29 cells were treated with PG3-Oc at the indicated concentrations for 48 h or 72 h, respectively. (E), (F), and (G) Dose-response and time-course analysis of cleavage of caspase-3, -8, cleaved PARP (cPARP), PUMA, and DR5 in PG3-Oc-treated HT29 cells or SW480 cells by western blot using the indicated antibodies. (H) Western blot analysis of active caspase-8, active caspase-3 and cleaved PARP in HT29 and SW480 cells. (I) HT29 cells were co-treated with 1 μM PG3-Oc and the pan-caspase inhibitor Z-VAD-fmk for 48 h. Sub G1 populations were analyzed by nuclear PI-staining using flow cytometry.

bioluminescent cell viability assay (Promega), following the manufacturer's protocol. Bioluminescence imaging was measured using the IVIS imager. Percentage of cell viability (mean \pm SEM) at each dose was calculated against the respective DMSO control. The IC₅₀ values were determined from the sigmoidal dose–response curves using GraphPad Prism.

Caspase activity assay

Cells were seeded in 96-well plate (1×10^4 cells/well). Cells were treated with different concentrations of compounds or DMSO as a control for 24 h. Caspase 3/7 activity was assessed by the Caspase-Glo 3/7 Assay kit (Promega), following the manufacturer's protocol. Bioluminescence imaging was measured using the IVIS imager. Caspase activity was normalized to cell numbers and compared to those of the DMSO treatment control in each cell line. Data is reported as mean RLU \pm SEM (n = 3).

Colony formation assays

Five hundred cells were seeded per well in 6-well plates and treated with different concentrations of compounds for 24 h, then, cells were cultured with drug-free complete medium for 2 weeks with fresh medium changed every 7 days. Cells were fixed with 10% formalin and stained with 0.05% crystal violet at the end of 2 wk period of cell culture [25].

Cell uptake and localization

A total of 5×10^4 cells was seeded in each well of 8-well chamber slides. Cells were incubated with PG3-Oc for 2 and 8 h respectively, washed and fixed by 4% paraformaldehyde for 15 min at room temperature, washed, stained with DAPI for 10 min, mounted, and examined by fluorescence microscopy.

Immunofluorescence staining

A total of 5×10^4 cells was seeded in each well of 8-well chamber slides. After treatment, cells were fixed and permeabilized by methanol:acetone (1:1) for 20 min at -20°C . Fixed cells were blocked by 2% BSA for 1 h, followed by primary antibody incubation for 1 h and Cy3-conjugated secondary antibody incubation for 1 h at room temperature. After washing, cells were stained with DAPI for 10 minutes at room temperature. Cells were mounted, and examined by fluorescence microscopy.

Flow cytometry assay

Cell Cycle Analysis—Propidium iodide staining and flow cytometry were used to determine the degree of cellular apoptosis. Cells were seeded at 3×10^5 cells/well in 6-well plates. Cells were treated with PG3-Oc for 48 h. Cells were harvested, fixed by 70% ethanol, and stained by propidium iodide, then flow cytometry was performed as previously described [28]. The percentage of hypo-diploid cells (sub-G1) was used to quantify dead cells in apoptosis assays.

qRT-PCR

Total RNA was isolated from PG3-Oc-treated cells using the Quick-RNA mini prep kit (Zymo Research, Irvine, CA) according to the manufacturer's protocol. 500 ng of total RNA was used to generate cDNA using SuperScript III first-strand synthesis system with random primers (Invitrogen), following manufacturer's protocol. Real-time PCR was performed using POWER SYBR GREEN mast mix (Applied Biosystem) for *DR5*, *p21*, *PUMA* and *GAPDH*, and TaqMan primer-probes for

detection of *MYC* mRNA levels on 7900HT Sequence Detection System (Applied Biosystem). *PUMA* primer (forward, 5'-GAC-GAC-CTC-AAC-GCA-CAG-TA-3'; reverse, 5'-AGG-AGT-CCC-ATG-ATG-AGA-TTG-T-3'), *DR5* primer (forward, 5'-ACAGTTGCAGCCGTAGTCTTG-3'; 5'-CCAGGTGCTTGTGAGCTTCT-3), *GAPDH* primer (forward, 5'-TCG ACA GTC AGC CGC ATC TTC TTT-3'; reverse, 5'-ACC AAA TCC GTT GAC TCC GAC CTT-3'), Taq Prob IDs for *MYC* (HS 00153408) and *GAPDH* (HS 99999905). $\Delta\Delta\text{Ct}$ method was used to analyze and report fold-changes of the indicated genes.

siRNA knockdown

Knockdown experiments were performed by transfecting either 80 pmoles of indicated siRNA(s), or scramble siRNA using RNAiMAX (Invitrogen). Transfected cells were treated with PG3-Oc, 24 hrs post-transfection. The control scrambled siRNA and siRNA for human ATF4, CHOP, DR5, Puma, NF- κ B p65, and MYC were purchased from Santa Cruz Biotechnology. p73 siRNA was from Ambion, and FOXO3a siRNA from Thermo Scientific Dharmacon.

Transfection of plasmids

Cells were transfected with *MYC* expression plasmids [26] and vector pcDNA3 (Invitrogen) using Lipofectamine 2000 (Invitrogen) according to the manufacturer's instruction.

RNA-Seq analysis

RNA-sequencing was performed by Fox Chase Cancer Center genomics facility (333 Cottman Ave, Philadelphia, PA 19111) and Genewiz (115 Corporate Boulevard, South Plainfield, NJ 07080). HT29 cells were treated with or without $1 \mu\text{M}$ PG3-Oc in triplicate for 24 h. HCT116 and HCT116 p53^{-/-} were treated with $50 \mu\text{M}$ 5-FU for 24 h. Total RNA was isolated using RNeasy Mini kit (Qiagen). RNA concentration and quality was analyzed using a NanoDrop 2000. RNA integrity of each sample was analyzed on a Bioanalyzer (Agilent).

Reagents: Truseq stranded mRNA library kit, HiSeq rapid SRcluster kit, HiSeq rapid SBS kit (Illumina,CA). Equipment: HiSeq2500 sequencer (Illumina, CA).

Stranded mRNA-seq library: 1000ng total RNAs from each sample were used to make library according to the product guide. In short, mRNAs were enriched twice via poly-T based RNA purification beads, and subjected to fragmentation at 94° for 8 min via divalent cation method. The first strand cDNA was synthesized by Superscript II and random primers at 42° for 15 mins, followed by second strand synthesis at 16° for 1 h. During second strand synthesis, the dUTP was used to replace dTTP, thereby the second strand was quenched during amplification. A single 'A' nucleotide is added to the 3' ends of the blunt fragments at 37° for 30 min. Adapters with illuminaP5, P7 sequences as well as indices were ligated to the cDNA fragment at 30° for 10 min. After Ampure bead (BD) purification, a 15-cycle PCR reaction was used to enrich the fragments. PCR was set at 98° for 10 sec, 60° for 30 sec and extended at 72° for 30 sec. Libraries were again purified using Ampure beads, had a quality check on bioanalyzer (Agilent) and quantified with Qubit (Invitrogen). Sample libraries were subsequently pooled and loaded to the sequencer. Single end reads at 100 bp were generated for the bioinformatic analysis.

Bioinformatics analysis: Pathway and network analysis (cut-off is 2-fold and above) by Ingenuity Pathway Analysis (IPA; Qiagen) was performed to identify key biological processes, canonical pathways, upstream transcriptional regulators and gene networks. Gene Set Enrichment Analysis was performed by ranking genes first by highest to lowest log 2-fold change. The ranked gene list was then queried using GSEA software to known

Molecular Signature Database (MsigDB). Known pathways from curated databases and published studies that matched our gene signature were then reported in the analysis.

Proteomic analysis

Sample preparation for LC-MS/MS analysis

Cell pellets (HCT116, HCT116 p53^{-/-} and HT29) were lysed with a lysis buffer (8 M urea, 1 mM sodium orthovanadate, 20 mM HEPES, 2.5 mM sodium pyrophosphate, 1 mM β -glycerophosphate, pH 8.0, 20 min, 4 °C) followed by sonication at 40% amplification by using a microtip sonicator (QSonica, LLC, Model no. Q55) and cleared by centrifugation (14 000 \times g, 15 min, 15°C). Protein concentration was measured (Pierce BCA Protein Assay, Thermo Fisher Scientific, IL, USA) and a total of 100 μ g of protein per sample was subjected for trypsin digestion. Tryptic peptides were desalted using C18 Sep-Pak plus cartridges (Waters, Milford, MA) and were lyophilized for 48 h to dryness. The dried eluted peptides were reconstituted in buffer A (0.1 M acetic acid) at a concentration of 1 μ g/ μ L and 5 μ L was injected for each analysis.

The LC-MS/MS was performed on a fully automated proteomic technology platform [27], that includes an Agilent 1200 Series Quaternary HPLC system (Agilent Technologies, Santa Clara, CA) connected to a Q Exactive Plus mass spectrometer (Thermo Fisher Scientific, Waltham, MA). The LC-MS/MS set up was used as described earlier (Ahsan et al., 2017, *J Proteomics* 2017, 165: 69–74). Briefly, the peptides were separated through a linear reversed-phase 90 min gradient from 0% to 40% buffer B (0.1 M acetic acid in acetonitrile) at a flow rate of 3 μ L/min through a 3 μ m 20 cm C18 column (OD/ID 360/75, Tip 8 μ m, New objectives, Woburn, MA) for a total of 90 min run time. The electrospray voltage of 2.0 kV was applied in a split-flow configuration, and spectra were collected using a top-9 data-dependent method. Survey full-scan MS spectra (m/z 400–1800) were acquired at a resolution of 70,000 with an AGC target value of 3×10^6 ions or a maximum ion injection time of 200 ms. The peptide fragmentation was performed via higher-energy collision dissociation with the energy set at 28 normalized collision energy. The MS/MS spectra were acquired at a resolution of 17,500, with a targeted value of 2×10^4 ions or maximum integration time of 200 ms. The ion selection abundance threshold was set at 8.0×10^2 with charge state exclusion of unassigned and $z = 1$, or 6 to 8 ions and dynamic exclusion time of 30 s.

Database search and label-free quantitative analysis

Peptide spectrum matching of MS/MS spectra of each file was searched against the human database (UniProt) using the Sequest algorithm within Proteome Discoverer v 2.3 software (Thermo Fisher Scientific, San Jose, CA). The Sequest database search was performed with the following parameters: trypsin enzyme cleavage specificity, 2 possible missed cleavages, 10 ppm mass tolerance for precursor ions, 0.02 Da mass tolerance for fragment ions. Search parameters permitted variable modification of methionine oxidation (+15.9949 Da) and static modification of carbamidomethylation (+57.0215 Da) on cysteine. Peptide assignments from the database search were filtered down to a 1% FDR. The relative label-free quantitative and comparative among the samples were performed using the Minora algorithm and the adjoining bioinformatics tools of the Proteome Discoverer 2.3 software. To select proteins that show a statistically significant change in abundance between 2 groups, a threshold of 1.5-fold change with *P*-value (0.05) were selected.

Knock-out of PUMA by CRISPR/Cas9 gene editing

sgRNA design and plasmid construction

sgRNA targeted the exon 3 of PUMA gene, which contains sequence code for BH3 domain of PUMA. Two crRNAs introduced into lentiviral

vectors (pLentiCRISPR-E, Addgene #78852) which contains eSpCas9 and puromycin cassette.

Guide1 DNA (forward, 5'-CACC GCGGGCGGTCCACCCAGG-3'; reverse, 5'-AAAC CCTGGGTGGGACCGCCCGCC-3') and Guide 2 DNA (forward, 5'-CACC GCCGCTCGTACTGTGCGTTG-3'; reverse, 5'-AAAC CAACGCACAGTACGAGCGGC-3') were annealed and ligated to the restriction enzyme-cut plasmid by T4 ligase. Stbl3 strain (Invitrogen C7373-03) was transformed by the guides-containing plasmids. LB-amp plates were streaked and incubated on a shaker at 37 °C overnight. The bacterial colonies were selected and mixed up with LB (Terrific Broth) and 100 μ g/mL ampicillin, and were incubated on a shaker at 37 °C overnight. Plasmids from different colonies were isolated and purified using QIAprep Spin Miniprep Kit (Qiagen). Plasmids were digested with BsmBI and BamHI in Cut Smart Buffer (New England BioLabs, Inc.) at 37 °C for 1 h and then analyzed by 1% agarose gel. Sequencing was performed by GENEWIZ (South Plainfield, New Jersey, NJ; Fig. S5 A–F).

Cell culture and DNA transfection

Lentivirus was generated with psPAX2, pVSV-G and the pLentiCRISPR plasmids that contain the guides and Cas9 in 293T cells. Forty-eight hours later, all supernatant was transferred to a 1.5 mL tube that was centrifuged to remove debris. The supernatant was transferred to a new 1.5 mL tube, and stored at 4 °C. HT29 cells were transfected with the lentivirus supernatant and polybrene was added to enhance the transfection. PuroMYCin (final concentration is 1 μ g/mL) was added to the medium to select positive cells.

Mutation screens by Sanger sequencing and TIDE analysis

DNA was extracted and purified from positive HT29 cells using DNeasy Blood & Tissue kit (Qiagen). PCR primers that flank both sides of the exon 3 of PUMA gene were used to amplify the target region (forward, 5'-CACAGTCTCTGGCCTTCTGG-3'; reverse, 5'-AGCTGCCGCACATCTGG-3'). The amplicon is GC-rich region, to improve PCR specificity, we performed temperature gradient PCR to optimize annealing temperature. A hot-start and touch-down PCR with accuPrime Pfx DNA Polymerase (ThermoFisher Scientific) and 2.5% DMSO and 1M betaine, was performed to achieve specific amplification of target region. The PCR products were purified by QIAquick PCR purification kit (Qiagen) for Sanger sequencing. TIDE analysis was performed using an online tool (TIDE: Tracking of Indels by DEcomposition, <https://tide-calculator.nki.nl/>). Sequencing was performed by GENEWIZ (South Plainfield, New Jersey, NJ; Fig. S5 C).

Single cell colonies

Three hundred positive HT29 cells were placed into a 10 cm dish and incubated at 37 °C. After 2 wk, single cell colonies were selected and expanded. Western blotting using PUMA antibody was performed to screen the colonies (Fig. S5 E and F).

In vivo antitumor assay and Immunohistochemistry

All animal experiments were approved by the Institutional Animal Care and Use Committee at Fox Chase Cancer Center and Brown University. One million HT29 or HCT116 p53^{-/-} cells were implanted subcutaneously in the flanks in each athymic nude mouse (female, 5–6 wk old). The mice with HT29 tumor xenografts were divided at random into 2 groups and treated with the vehicle (10% DMSO, 20% Kolliphor EL in PBS) and PG3-Oc (5 mg/kg, 3 times/wk) by intraperitoneal injection when the tumor masses reached a size of 5 to 6 mm (Supplemental Fig. S9 A). The mice with HCT116 p53^{-/-} tumor xenografts were divided at random into 2 groups and treated with the vehicle (10% DMSO, 20% Kolliphor EL in PBS) and PG3-Oc•HCl (7.6 mg/kg/day) by intraperitoneal injection when the tumor masses reached a size of 5 to 6 mm (Fig. S9 H and J). Subsequently tumor volumes

Table 1

IC₅₀ values for different cancer cell lines with various mutant p53 status.

Tumor/Tissue Type	Cell Line	IC ₅₀ (nM)	P53 Status
Colorectal Cancer	HT29	66.3	R273H
	SW480	95.3 (4-fold)	R273, P309S
	DLD1	54	S241F
	HCT116 p53 ^{-/-}	41.1(9 fold)	Null
Nontransformed colorectal epithelial cells	CCD 841 Con	375.2	WT
	Head & neck squamous cell carcinoma	FaDu	R248L
	CAL-27	33.9	H193L
Pancreatic Cancer	PANC-1	135.5	R273H
	ASPC-1	39.2	Frameshift
Breast Cancer	MDA-MB-231	242.3	R280K
	MDA-MB-468	97.6	R273H
Glioblastoma Multiforme	U251	100.2	R273H
	NSCLC	H1975	R273H

were measured with a caliper and calculated using $V = 0.5 \times \text{Length} \times \text{Width}^2$. Twenty-three days after treatment, the mice were euthanized and tumors were excised. H&E staining and Immunohistochemistry (IHC) of paraffin-embedded tumor and tissue sections were performed at the Fox Chase Cancer Center Histopathology Facility and Brown University Alpert Medical School Molecular Pathology Core. Antibodies for IHC: PUMA (Santa Cruz Biotechnology), Ki-67, DR5 and cleaved Caspase 3 (Cell Signaling Technology), ATF4 (Abcam).

Statistical analysis

All results were obtained from triplicate experiments, unless other indicated. Statistical analyses were performed using PRISM4 Software (GraphPad Software, Inc.), and the Student *t* test. Statistical significances were determined by $P < 0.05$.

Results

PG3-Oc inhibits cell proliferation and induces apoptosis in mutant p53-expressing cancer cell lines

As a candidate p53-pathway restoring compound with an undefined mechanism of action, PG3-Oc (Fig. 1A) is a potent inhibitor of cell proliferation and is efficacious in a broad spectrum of human cancer cells with mutant p53, with IC₅₀ values within the nano-molar range (Table 1). PG3-Oc has a 4- to 9-fold therapeutic index in colorectal cancer cell lines as compared to normal colon cells CCD 841 Con (Fig. 1B and Table 1). In addition, PG3-Oc has antiproliferative effects on other tumor cell types, including head and neck squamous cell cancer cell lines, pancreatic cancer, breast cancer, glioblastoma multiforme, and non-small cell lung cancer cell lines (Fig. 1C and Table 1). Similar to CRC, the IC₅₀ in additional tumor types is also in the sub-micromolar range (Table 1). Over 90% inhibition in long-term cell proliferation is also observed in a panel of CRC cell lines treated with low dose PG3-Oc (Fig. S1 A and B). Treatment with PG3-Oc induces a 2-fold increase in caspase 3/7 activity as compared to untreated cells using mutant p53-expressing and p73-null cancer cells (Fig. S1 C). PG3-Oc's apoptotic activity is p73-independent as evident by the comparable caspase 3/7 activity in both p53 mutant DLD1 and DLD1-p73^{-/-} cells post PG3-Oc treatment (Fig. S1 C). Treatment of colorectal cancer cell lines HT29 and SW480 with PG3-Oc induces cancer cell death in a dose-and-time dependent manner as demonstrated by sub-G1 analysis (Fig. 1D, Fig. S1 D and E).

To evaluate if the cell death is caspase-dependent, apoptosis markers were analyzed by western blot. As seen in Fig. 1E, as low as 0.5 μM PG3-Oc is sufficient to activate cleaved caspase-8 and -3 and cleaved-PARP in HT29

cells. Time-course experiments indicate that PUMA protein is first induced at 16 h post PG3-Oc treatment and this induction is sustained even at 48 h. At 48 h, we note that induction of cleaved PARP, as well as cleaved caspase-8 and -3 occur in both HT29 and SW480 CRC cell lines (Fig. 1F and G). These data also clearly indicate that PG3-Oc induces upregulation of PUMA and DR5 in a dose- and time-dependent manner.

Caspase-dependent induction of apoptosis was further confirmed by the pan-caspase inhibitor (Z-VAD-FMK) co-treatment experiments with PG3-Oc. Western blot analysis show that Z-VAD-FMK completely inhibits the cleavage of caspase-8 and caspase-3 in both HT29 and SW480 cells (Fig. 1H). Under the same experimental conditions, 20 μM Z-VAD-FMK completely blocks the formation of a sub-G1 population as compared to the untreated control (Fig. 1I). Taken together, these data suggest that PG3-Oc treatment induces caspase-8 and caspase-3 activation in CRC cell lines, and caspase activation is required for PG3-Oc-induced cell death.

PG3-Oc partially restores global p53 pathway signaling

Having confirmed that PG3-Oc induces apoptosis in multiple mutant p53-expressing cancer cell lines, we investigated whether this small molecule restores the p53 signaling pathway more globally in p53-mutant HT29 and HCT116 p53^{-/-} cells after treatment with 1 μM PG3-Oc for 24 h. Meta-analysis approaches that enabled comparisons of multiple genome-wide data sets of p53 binding and gene regulation revealed that (1) the transcription factor p53 itself is solely an activator of transcription, (2) gene downregulation by p53 is indirect and requires p21 [10]. Therefore, we focused on upregulated p53 target genes to assess p53 pathway restoration.

Initially, we investigated whether PG3-Oc induces key p53 target genes that regulate cellular apoptosis by qRT-PCR and Western blot. HT29 cells were treated with 1 μM PG3-Oc at different time points followed by qRT-PCR analysis. Time-dependent induction of DR5 (Death Receptor 5), p21 and PUMA (P53-Upregulated Mediator of Apoptosis) transcripts is observed in PG3-Oc treated cells (Fig. 2A). Importantly, PG3-Oc very strongly induces upregulation of PUMA mRNA in all 3 cell lines at the 8- or 19-h time points (Fig. 2A-C). Over a 3-fold induction of p21 mRNA is observed at 8 and 19 h post-treatment with PG3-Oc in HT29 and HCT116 p53^{-/-} cells, but no significant change is observed in SW480 cells. For the DR5 mRNA level, approximately a 2-fold upregulation at 19 h post-treatment is observed in HT29 and SW480 cells, but not in HCT116-p53^{-/-} cells (Fig. 2A-C).

Western blot analysis of p53-mutant DLD1, SW480, HT29 cells, and HCT116-p53^{-/-} colon cancer cells show strong upregulation of DR5, p21, PUMA, and Noxa (Phorbol-12-Myristate-13-Acetate-Induced Protein 1) in a time- and dose-dependent manner (Fig. 1E-G; Fig. 2 D-F), which is consistent with the qRT-PCR results.

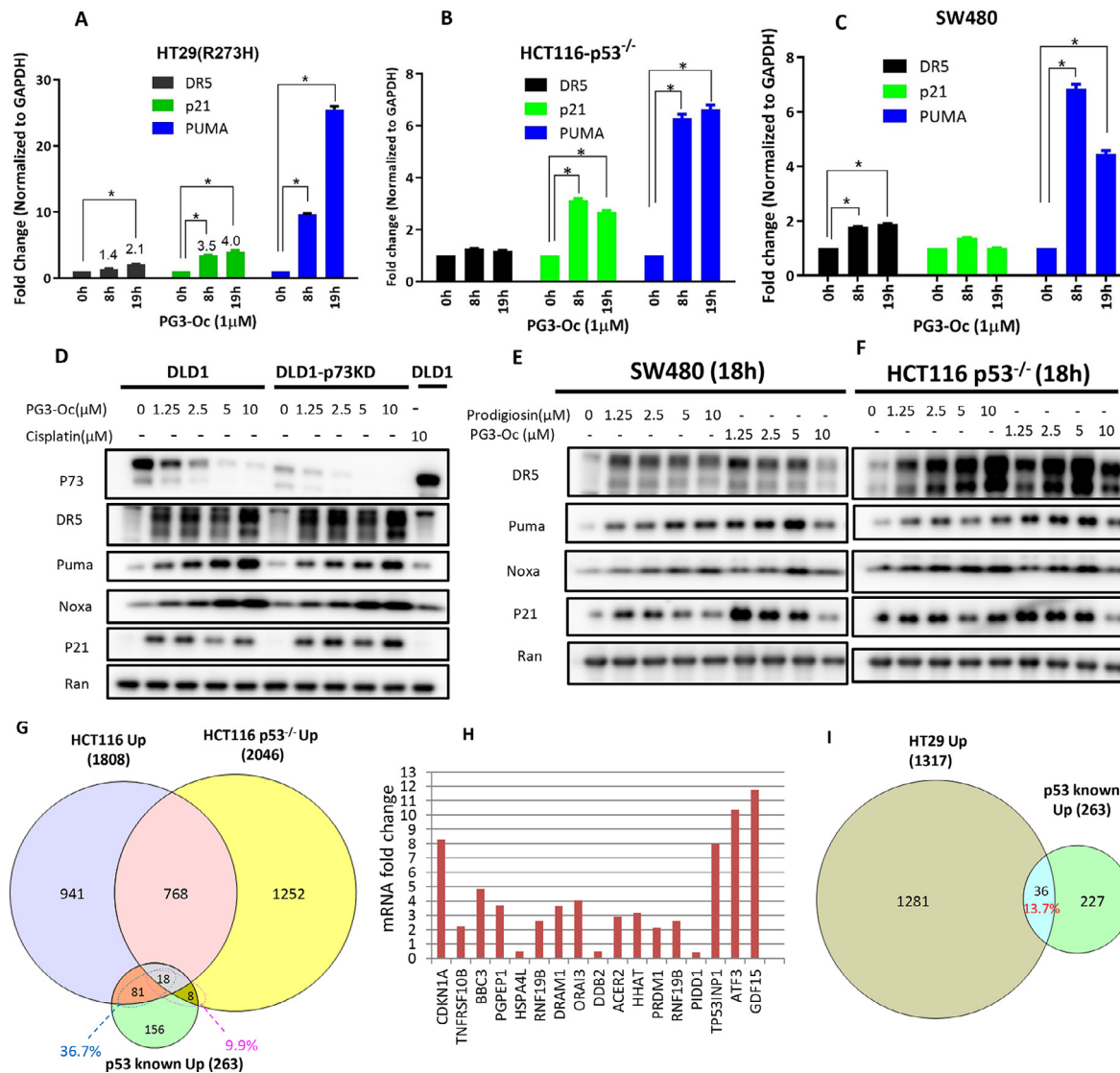


Fig. 2. PG3-Oc partially restores the p53 pathway globally. (A), (B), and (C) Cells were treated with 1 μM PG3-Oc for 8 and 18 h. qRT-PCR analysis of the change of mRNA level in HT29 and HCT116 p53^{-/-} and SW480 cells. mRNA samples were prepared and RT-PCR was performed to prepare cDNAs as described in Materials and Methods. (D), (E), and (F) Western blot analysis of p53-target gene expression of DR5, PUMA, Noxa, and p21 in p53-mutant and p53-null cancer cells. Cells were treated with the indicated doses of PG3-Oc for 18 h. (G) HCT116 and HCT116 p53^{-/-} cells were treated with/without 50 μM 5-FU for 24 h in triplicate, and RNA samples were prepared. RNA-seq were performed. Venn diagram shows that 5-FU induced p53 target gene expression. (H) HT29 cells were treated with or without 1 μM PG3-Oc for 24 h in triplicate, and RNA samples were prepared. Gene differential expression were measured by RNA-Seq (FDR = 5%). A subset of typical p53 target genes were positively regulated by PG3-Oc. (I) HT29 cells were treated with or without 1 μM PG3-Oc for 24 h in triplicate, and RNA samples were prepared. RNA-Seq, IPA and GSEA were performed (see Materials and Methods for details). Venn diagram shows that PG3-Oc restores p53 target gene expression partially. (J) Common genes between 99 p53 target genes induced by 5-FU from G and 36 p53 target genes induced by PG3-Oc from H. (K) GSEA plot: Representative gene set from 1867 differential expression genes showing specific responses to the p53 pathway. (L) and (M). Proteomic identification of PG3-Oc responsive p53 restored protein in HCT116-p53^{-/-} and HT29 cell lines. Cells were treated with 1 μM PG3-Oc for 8, 16, and 24 h. Venn diagram analysis were performed in comparison with the in-house build p53 dependent gene (proteome) and known 53 gene data-base. (N) KEGG gene enrichment analysis of the overlapped p53 restored proteins identified from proteome analysis (L and M). As expected, the p53 signaling pathway proteins were top hit. In addition, proteins associated with cancer, MAPK signaling, and apoptosis signaling pathway were highly enriched. (O) Heat map analysis of genes identified by proteomic analysis of HCT116-p53^{-/-} (Proteo: Proteomics), HT29 (Proteo: Proteomics) and transcriptome analysis of HCT116 in response to PG3-Oc treatment (Trans: Transcriptome). Proteins were selected from the KEGG gene enrichment pathway analysis in N.

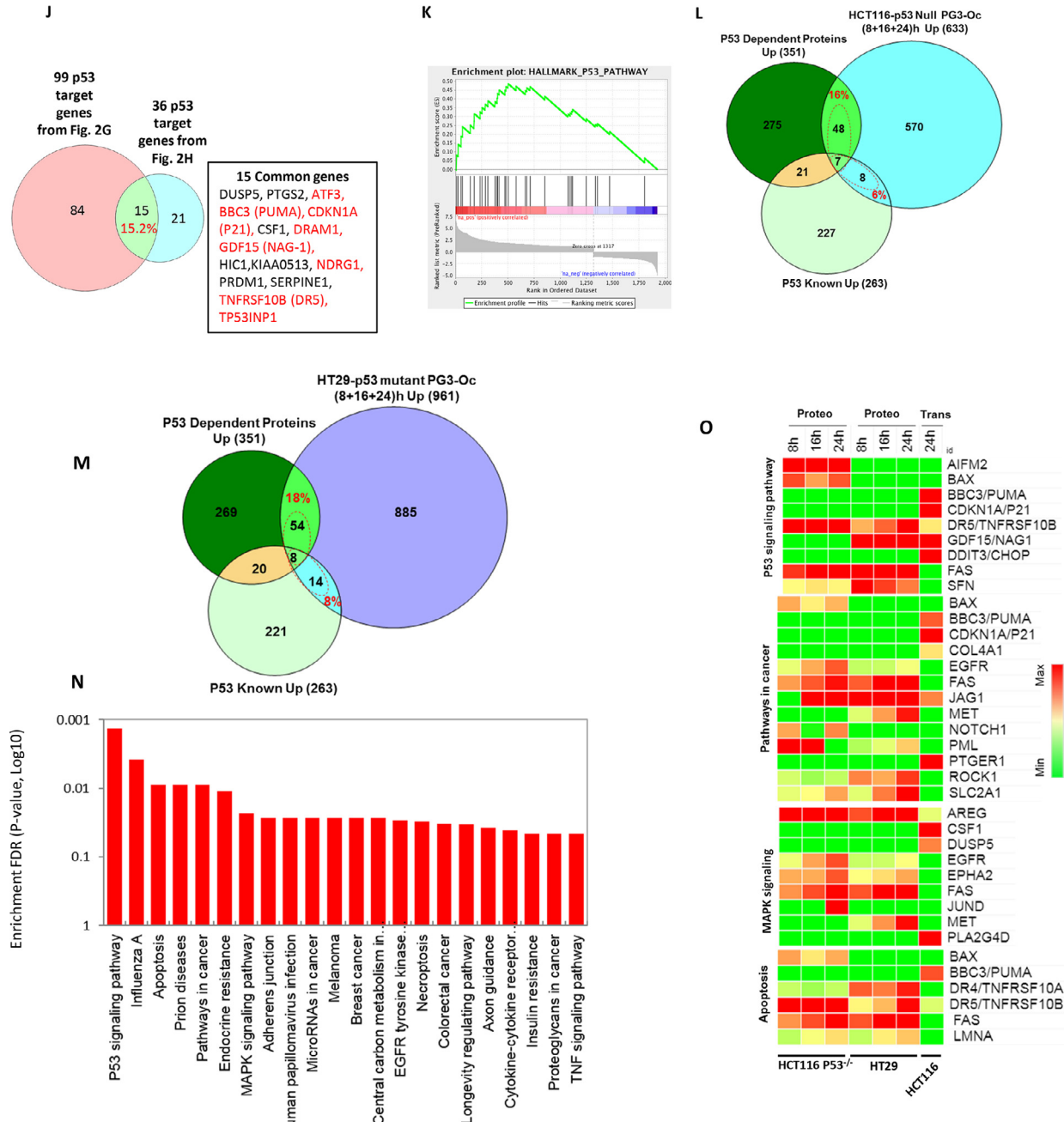


Fig. 2. Continued

In order to develop a reference p53 target/responsive gene collection as a control, HCT116 cells and HCT116 p53^{-/-} cells were treated with 50 μM of the p53 activator 5-Fluorouracil (5-FU) for 24 and 48 h. Western blot indicates that a set of typical p53 target genes (p21, PUMA, DR5, NAG-1, and Noxa) is significantly upregulated over time in HCT116 cells, whereas their expression is not changed in HCT116 p53^{-/-} (Fig. S2 A). Then, isogenic HCT116 and HCT116 p53^{-/-} cells were treated with or without 50 μM 5-FU for 24 h in triplicate, RNA samples were prepared and RNA-seq was performed (Supplemental Files S1–S3). Principal component analysis shows close clustering of total normalized mRNA abundance of the replication in each condition, however, each treatment condition is significantly distinct from other groups (Fig. S2 B and C). The global change in transcription across the groups compared is visualized by a volcano plot

(Fig. S2 D and E). IPA revealed that the p53 pathway is a top hit and is activated in HCT116 cells, but not in HCT116 p53^{-/-} cells (Fig. S2 F and G). GSEA (gene set enrichment analysis) show that p53 signaling pathway is a top hit and the most enriched pathway in HCT116 cells, but not in HCT116 p53^{-/-} cells (Fig. S2 H–J). Not surprisingly, the “p53 pathway” is a top hit found in both IPA and GSEA analyses.

Fischer’s p53 target gene set contains a total of 344 including 263 genes positively regulated by p53 and 81 genes negatively regulated by p53 [10]. The total of 344 and 263 genes is found in a spreadsheet in supplementary data (Supplementary Table S1 in the Fischer manuscript) rather than the total of 346 and 246 genes referred to in the text of the manuscript [10]. As Fig. 2G shows, compared to known p53 target gene data base (263 positively regulated genes only), 5-FU induced upregulation of 99 (81+18) p53 target

genes in p53 wild-type HCT116 (cutoff of fold change = 1.87, FDR 0.05), which covers 37.6% (99/263) of the p53 target gene database. Though p53 is a *bona fide* transcription factor of p53 target genes, this data clearly indicates that 5-FU through DNA damage partially restores the p53 pathway in p53 wild-type HCT116 cells. By contrast, in HCT116 p53^{-/-} cells, 26 p53 target genes were upregulated, which is p53-independent. This represents 9.9% (26/263) restoration of p53 target genes through unknown transcription factors in p53-deficient cells treated with 5-FU. These results are consistent with the notion that transcription programs by p53 are dependent on cell-type, as well as the nature of the stresses and inducers.

HT29 cells were treated with or without 1 μ M PG3-Oc for 24 h. RNA samples were prepared, and then RNA-Seq was performed (Supplemental Files S4). Key p53 target genes *CDKN1A* (p21), *TNFRSF10B* (DR5), *BBC3* (PUMA), *TP53INP1* (Teap) and *GDF15* (NAG-1) are significantly upregulated (Fig. 2H) and identified in IPA canonical p53 pathway analysis (Fig. S2 K and L). IPA analysis (cutoff of log₂ fold change = 2, FDR 0.05) of 1317 up-regulated genes revealed that among the 263 known p53 target genes, 36 genes are up-regulated (Fig. 2I). That is 13.7% (36/263) of 263 total p53 genes, and higher than 9.9% of 5-FU-induced restoration of the p53 target genes in HCT116 p53^{-/-} cells.

There are 15 overlapping p53 target genes between the 99 genes induced by 5-FU from Fig. 2G and the 36 genes induced by PG3-Oc from Fig. 2I as shown in a Venn diagram analysis (Fig. 2J), which covers 15.2% (15/99) of 99 5-FU-induced p53 target genes (Fig. 2J). Importantly, the analysis indicates that critical effector p53 target genes that are involved in cell cycle arrest (p21), apoptosis (PUMA, DR5, Noxa, and NAG-1), autophagy (DRAM1), and suppression of cancer cell metastasis (NDRG1) are in this overlapping gene set and are potently induced (Fig. 2J, highlighted in red). These data suggest that although the percentage of restoration of p53 target genes is dependent on both cell type and nature of inducers, the p53 core gene set that regulates cell proliferation and apoptosis could be induced regardless of cell type and properties of inducers in tested cell lines.

GSEA analysis indicates that PG3-Oc-induced differential expression of genes is enriched in the p53 pathway (Fig. 2K), suggesting PG3-Oc has a significant impact on upregulation of p53 target genes in p53-mutant cells. Also, the apoptosis signaling pathway is highly enriched in PG3-Oc treated tumor cells (Fig. S2 M).

Because very limited information is available on the proteomic changes in p53 mutant and p53-null cell lines, we investigated the proteomic response of HCT116 and HCT116 p53^{-/-} cell lines treated with or without 50 μ M 5-FU for 24 h (Fig. S3 A–E). In a comparative analysis, a total of 448 proteins are increased in abundance at least 1.5-fold in response to 5-FU in the HCT116 cell line whereas 455 proteins are increased in the HCT116 p53^{-/-} cell line. A comparison of these 2 proteome sets showed 283 proteins are unique in the HCT116 cell line whereas 165 proteins are overlapping with the p53-null cell line (Fig. S3 F). Enrichment analysis indicates that p53-regulated metabolic signaling was significantly enriched in HCT116 cells, but not in HCT116 p53^{-/-} cells (Fig. S3 G and H). Among these overlapping proteins, 68 show increased abundance of at least 1.2-fold in HCT116 cells as compared with the p53-null cell line. Thus, a total of 351 (283 + 68) proteins are considered as our p53-responsive proteome dataset (Fig. 2L) which we further use as a positive p53 control proteome for comparison with PG3-Oc treatment of the HT29 and HCT116-p53^{-/-} cell lines (Supplementary Table 2).

To evaluate the restoration of p53-dependent proteins in HCT116 p53^{-/-} and mutant p53-expressing HT29 cell lines in response to PG3-Oc treatment, the cell lines were exposed to 1 μ M PG3-Oc treatment for 8, 16, and 24 h and subjected to proteomic analysis, respectively (Fig. S3 I–M). Because expression of p53 target genes is also time-dependent, genes upregulated at any of the 3 timepoints (8, 16, and 24 h) were included. A total of 633 (Fig. 2L) and 961 (Fig. 2M) proteins were increased at least 1.5-fold in response to PG3-Oc treatment in HCT116 p53^{-/-} and

HT29 cells, respectively (Fig. 2L, M and Supplementary Tables 3 and 4). These protein sets were further compared with our reference p53-responsive proteome dataset (Fig. 2L, M and Supplementary Table 2). Venn diagram analysis shows that 16% (55/351) of the p53-responsive proteins are restored in the HCT116-p53^{-/-} cell line in response to 1 μ M PG3-Oc treatment as compared with our reference p53-responsive proteome dataset. An additional 6% (15/263) of upregulated proteins are overlapping with the known p53 target gene database (Fig. 2L). Similarly, 18% (62/351) proteins are restored in the mutant p53-expressing HT29 cell line when compared with our reference p53-responsive proteome dataset and an additional 8% (22/263) are overlapping with the known p53 target gene dataset (Fig. 2M). This analysis suggests that proteomic analysis of p53 pathway restoration is feasible and the percentages of p53 target genes restored by PG3-Oc in the HT29 cell line are similar: 13.7% in the transcriptome and 18% in the proteome analysis (Fig. 2I and M).

KEGG gene enrichment analysis of the overlapping p53 restored proteins identified from Fig. 2L and M proteome analysis found that the p53 signaling pathway is a top hit (Fig. 2N), suggesting PG3-Oc is able to restore proteins of p53 target genes partially, which is consistent with the transcriptome analysis.

We performed a heat map analysis of restored p53 pathway genes identified by proteomic analysis of HCT116 p53^{-/-} and HT29 cell lines in response to PG3-Oc treatment (Fig. 2O). Proteins were selected from the KEGG gene enrichment pathway analysis in Fig. 2N (Supplementary Table 6). Proteins associated with cancer, MAPK signaling, and apoptosis signaling pathways are highly enriched (Fig. 2O).

Taken together, these data suggest that PG3-Oc can partially restore the p53 pathway in mutant p53-expressing HT29 and p53-null HCT116 cancer cell lines at both the transcriptional and protein levels.

PUMA is required for PG3-Oc mediated cell death

PUMA is a BH3-only Bcl-2 family member that binds and inactivates anti-apoptotic proteins like Bcl-2, Bcl-X_L, and Mcl-1. This facilitates induction of the caspase-9 mediated intrinsic apoptosis pathway [28,29]. DR5 activation results in recruitment of the adaptor protein FADD (Fas-associated death domain) and caspase-8 to form the DISC (death inducing signaling complex), leading to the cleavage and activation of caspase-8. Activated caspase-8 can directly activate effector caspase-3/7 via the extrinsic pathway (Type I) or cleave Bid (BH3 interacting-domain death agonist) and activate the intrinsic pathway (Type II), leading to cell apoptosis [29,30]. Since PUMA and DR5 are important proapoptotic proteins, we evaluated if PUMA and DR5 are dispensable for PG3-Oc mediated cell death in mutant p53-expressing cells. As shown in Fig. 3A, when PUMA was knocked down, alone or together with DR5, using siRNA, there was complete blunting of PARP cleavage and cleavage of caspases after PG3-Oc treatment. Similar results were observed when knockdown of PUMA by siRNA reduced the sub-G1 population to 11.1% as compared to 25.8% in siControl, in PG3-Oc treated cells (Figs. 3B and S4 A). DR5 knockdown alone had no impact on the same apoptotic markers and Sub-G1 population under the experimental conditions (Figs. 3A, B and S4 A). However, our preliminary data shows that PG3-Oc-induced upregulation of DR5 sensitizes TRAIL-resistant HT29 cells to TRAIL treatment (Fig. S4 C–E).

PUMA siRNA studies were validated by creating *PUMA* gene knockout HT29 cells via CRISPR/Cas9 gene-editing technology (Fig. S5, for details see Materials and Methods). The gRNA was designed to target the DNA sequence that encodes amino-acid residues for the BH3-domain of PUMA (Fig. S5 A). Knockout of the *PUMA* gene abolishes PG3-Oc-induced cleavage of PARP and caspase-8, -3 and the sub-G1 population, which was the same as the positive control caspase-8 inhibitor Z-IETD-fmk and the pan-caspase inhibitor Z-VAD (Figs. 3C and D and S4 B). Taken together, these data suggest PUMA protein is required and is a key mediator in cell death induced by PG3-Oc treatment in HT29 cancer cells.

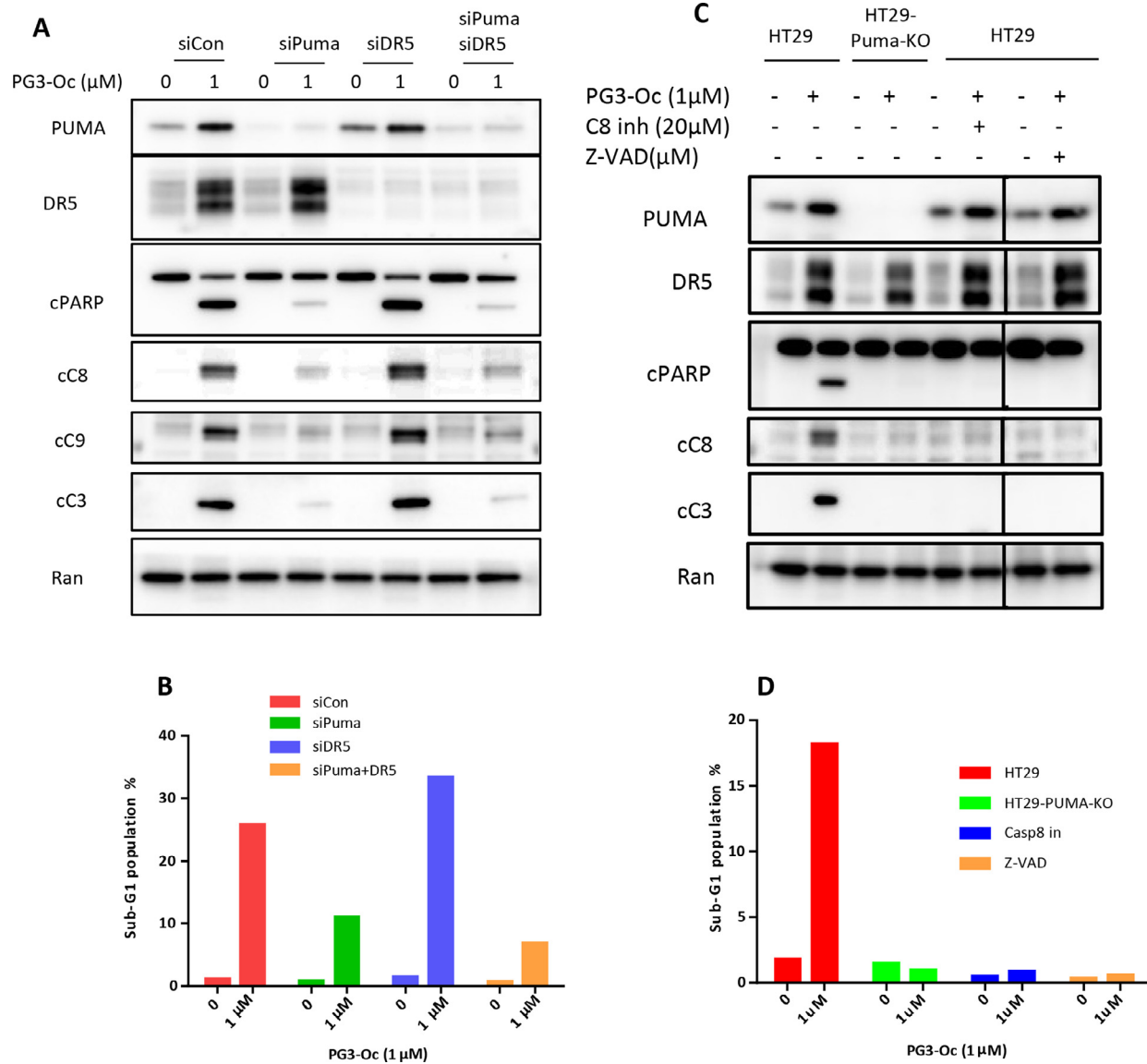


Fig. 3. PUMA is required for PG3-Oc-mediated cell death. (A) HT29 cells were transfected with Control, PUMA, DR5, and PUMA/DR5 siRNAs, and at 24 h after transfection, the cells were treated with 1 μM PG3-Oc for 48 h. After treatment, western blot analysis of PUMA, DR5, cleavage of caspase-8, -3, -9, and cleaved PARP was performed using indicated antibodies. (B) Cell death was analyzed by nuclear PI-staining using flow cytometry. (C) HT29 and HT29-PUMA-KO cells were treated with PG3-Oc or co-treated with the caspase 8 inhibitor (cas8 inh) or pan-caspase (Z-VAD-FMK) inhibitor for 48 h. Cleavage of caspases and PARP were detected by western blotting using the indicated antibodies. (D) Sub G1 populations were analyzed by flow cytometry.

Of note, both knockdown and knockout of the *PUMA* gene abolishes caspase-8 and caspase-3 cleavage/activation and PARP cleavage after PG3-Oc treatment (Fig. 3A and C). Furthermore, the caspase-8 inhibitor Z-IETD-fmk not only inhibits caspase-8 cleavage, but also results in inhibition of caspase-3 and PARP cleavage. Knockdown of caspase-8 using caspase-8 siRNA blocked PG3-Oc-induced cleavage of PARP (Fig. S4 D) and greatly reduced the formation of Sub-G1 population (Fig. S4 E). These data suggest that the induced PUMA is able to feedback to mediate the activation of caspase-8 through an unknown mechanism.

PG3-Oc dependent repression of MYC upregulates PUMA

PG3-Oc-induces significant downregulation of MYC and upregulation of PUMA protein levels is observed in a panel of p53 mutant cell lines, such as HT29, DLD1, FaDu, MDA-MB-231, and MDA-MB-468. SW480 and CAL27 showed slight downregulation of MYC (Fig. 4A). Inhibition of MYC

leads to downregulation of expression of its target gene E2F1, and inhibition of expression of E2F1 target gene p73 (Fig. 4B). Transcriptome data analysis in HT29 cells also shows that PG3-Oc treatment downregulates E2F1 and p73 mRNA levels as compared to untreated control cells (Fig. S 2K and 2L). Experiments in isogenic HCT116 cells with wild-type p53 or p53^{-/-} cells show no significant differences in induction of PUMA or downregulation of MYC by PG3-Oc (Fig. 4C). Taken together, these data suggest that PG3-Oc-induced downregulation of MYC and upregulation of PUMA is not limited to a specific cell line or p53 mutation, and is independent of p53 status.

It was reported that MYC binds to the *PUMA* promoter and represses *PUMA* gene transcription [31,32]. We explored whether PG3-Oc-induced downregulation of MYC activates *PUMA* gene transcription. Basal PUMA levels are modestly de-repressed on knockdown of MYC, both at the protein and mRNA levels (Fig. 4D and E). Over-expression of MYC leads to attenuation of PUMA induction at both the protein and mRNA levels (Fig. 4F and G) post PG3-Oc treatment. Because the fold changes of qRT-

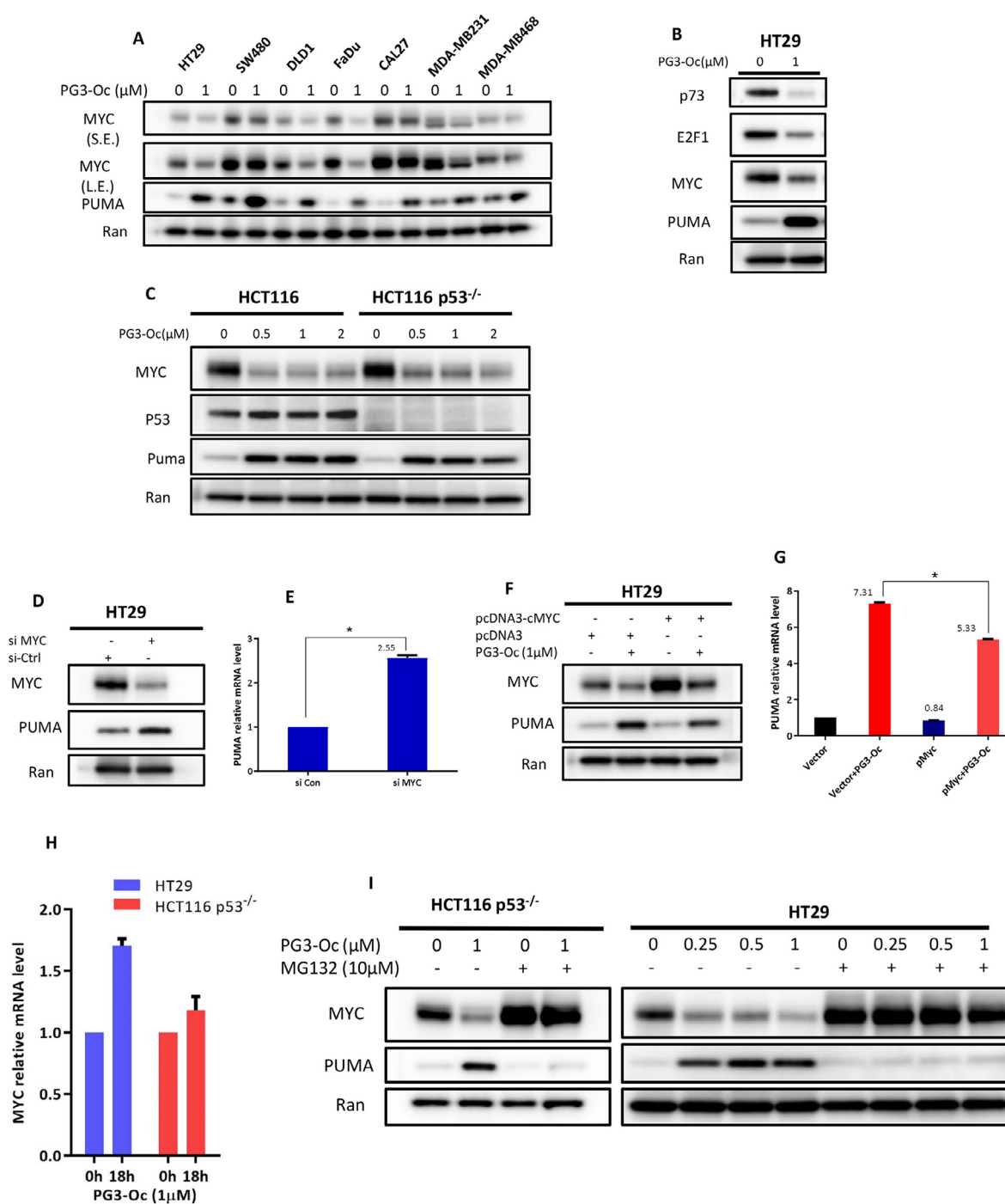


Fig. 4. PG3-Oc dependent repression of MYC upregulates PUMA. (A) Various mutant p53-expressing cancer cell lines were treated with PG3-Oc for 24 h. Cell lysates were prepared for western blots using the indicated antibodies. S.E.: short exposure; L.E.: long exposure. (B) HT29 cells were treated with 1 μ M PG3-Oc for 24 h, and western blots were performed using the indicated antibodies. (C) HCT116 and HCT116 p53^{-/-} cells were treated with PG3-Oc at the indicated doses for 24 h, and western blots were carried out by using the indicated antibodies. (D) Cells were transfected with MYC siRNAs and control siRNAs for 48 h, cell lysates were prepared for western blots, and (E) mRNAs were extracted for qRT-PCR analysis to evaluate the change of PUMA mRNA levels after PG3-Oc treatment. (F) HT29 cells were transfected with the vector pcDNA3 and pcDNA3-cMYC, and after 24 h, cells were treated with 1 μ M PG3-Oc for 17 h. Cell lysates were prepared for western blots. (G) mRNA was extracted for qRT-PCR analysis to determine the change of PUMA mRNA levels after PG3-Oc treatment. (H) HT29 and HCT116 p53^{-/-} cells were treated with PG3-Oc for 18 h, and mRNAs were extracted for cDNA synthesis and qRT-PCR analysis to determine the change of MYC mRNA levels after PG3-Oc treatment. (I) Cells were co-treated with the proteasome inhibitor MG132 for 24 h, and western blot was performed with the indicated antibodies. (J) Analysis of MYC target genes from RNA-Seq analysis with differential gene expression induced by 1 μ M PG3-Oc after 24 h treatment in HT29 cells. (K) GSEA plot: Representative gene set from 1867 differential expression genes with specific response to MYC.

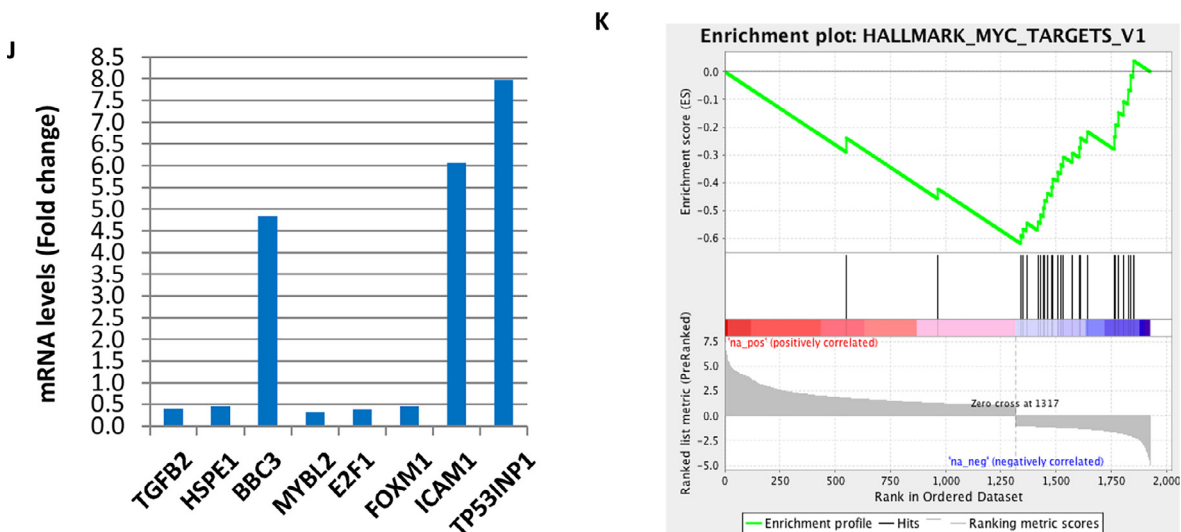


Fig. 4. Continued

PCR data should be above 2 fold for significant changes, these data indicates that PG3-Oc treatment does not significantly change MYC mRNA levels in either HT29 or HCT116 p53^{-/-} cell lines (Fig. 4H), suggesting MYC downregulation may be occurring through the proteasome pathway. To study whether endogenous MYC can inhibit PG3-Oc-induced upregulation of PUMA or not, HCT116 p53^{-/-} and HT29 cells were co-treated with PG3-Oc and proteasome inhibitor MG132. MG132 blocks MYC degradation and leads to accumulation of endogenous MYC that abolishes the PG3-Oc-induced upregulation of PUMA (Fig. 4I). Taken together, these data indicate that degradation of MYC allows PUMA gene expression, which is consistent with MYC negative regulation of PUMA expression [32,33]. MYC protein degradation occurs through the proteasome pathway in the tested cell lines.

RNA-Seq data of PG3-Oc-treated HT29 cells indicates that MYC-activated genes (Fig. 4J), *TGFB2* (TGF β -2), *HSPE1* (Hsp10), *MYBL2* (B-Myb), *E2F1* (E2F1), and *FOXM1* (FOXO1) [31], are downregulated. By contrast, MYC-repressed genes, *BBC3* (PUMA), *ICAM1* (ICAM1), and *TP53INP1* (TP53INP1) [32,33], are upregulated (Fig. 4J). GSEA analysis indicates that downregulation of genes is enriched in the MYC pathway, suggesting that PG3-Oc has a significant negative impact on the MYC pathway and network (Fig. 4K).

In summary, our data demonstrate that PG3-Oc-induced degradation of MYC correlates well with subsequent upregulation of PUMA in the tested cell lines.

ATF4 is a key regulator that mediates PG3-Oc-induced p53 pathway restoration

We sought to discover upstream regulators that mediate p53 pathway restoration in mutant p53-expressing cancer cells following PG3-Oc treatment. We also questioned which transcription factor may positively regulate *PUMA* gene expression after MYC degradation. Transcription factors p73 is a p53 family member, and the majority of the genome-wide p53 target sites can be bound by p73 in vivo [34]. p73 binds to p53-responsive elements and regulate *PUMA* gene expression in response to various stressful stimuli [35,36]. However, in this case, we observed that PG3-Oc treatment leads to downregulation of p73 both at the protein level (Figs 2D and B) and the mRNA level (Fig. S2 K and L). Consistent with this, induced upregulation of DR5, p21, PUMA, and Noxa between DLD1 and DLD1-p73^{-/-} cell lines show no significant differences (Fig. 2D). To further verify these observations, siRNA knockdown of p73 was performed, and was found to not attenuate

PG3-Oc-induced upregulation of PUMA in HT29 cells (Fig. S6 A). Thus, the upregulation of the p53 pathway by PG3-Oc is independent of p73.

Transcription factors FOXO3a, NF- κ B, and JNK/c-Jun can regulate *PUMA* gene expression in a p53-independent manner depending on cell type and stimuli [37–43]. Knockdown of transcription factors NF- κ B (p65), or inhibition of JNK/c-Jun signaling by JNK inhibitor SP600125 does not blunt PG3-Oc-induced upregulation of PUMA (Fig. S6 B and C). These data suggest that NF- κ B and JNK/c-Jun are not involved in the regulation of PUMA in PG3-Oc-treated cells. Knockdown of FOXO3a induced upregulation of PUMA level, therefore, it is difficult to know whether FOXO3a involved in the regulation of the response of PUMA to PG3-Oc (Fig. S6 B).

It was reported that PUMA, Noxa, p21 and NAG-1 are ATF4 direct target genes [20,41,44]. We found that knockdown of ATF4 not only blocks PG3-Oc induced upregulation of PUMA, but also DR5, p21, Noxa and NAG-1, as shown in Fig. 5A and B. Also, knockdown of ATF4 does not block PG3-Oc-induced downregulation of MYC, indicating after MYC degradation and de-repression of *PUMA* gene, it is ATF4 that mediates the expression of the *PUMA* gene (Fig. 5A and B). CHOP is an ATF4 direct target gene, and it directly regulates DR5, Noxa and PUMA gene expression [40,45,46]. We observed that knockdown of ATF4 leads to downregulation of CHOP (Fig. 5A and B), and knockdown of CHOP blocks PG3-Oc-induced upregulation of DR5 and Noxa, but not PUMA, p21 and NAG-1 (Fig. 5C and D). Taken together, these data suggest that ATF4 is an upstream regulator that mediates p53 pathway restoration induced by PG3-Oc in p53-deficient cells.

To further confirm our hypothesis, transcriptome analysis of siATF4-knockdown experiment was performed. HT29 cells were transfected with control or ATF4 siRNAs respectively, after 24 h, cells were treated with or without PG3-Oc for 24 h. RNA samples were prepared and RNA-Seq and IPA analysis was performed (cutoff of fold change = 2, FDR 0.05; Supplemental Files S5–S7). IPA canonical pathway analysis identified that the p53 signaling pathway is significantly activated in HT29 cells, but not in siATF4/PG3-Oc-treated HT29 cells (Fig. S7 A–C). The heatmap of signaling pathway and network analysis clearly indicate that p53 signaling is activated in siControl/PG3-Oc-treated HT29 cells, and inhibited in siATF4/PG3-Oc-treated HT29 cells (Fig. S7 D).

YW3-56 is a compound that induces ER stress in the triple negative breast cancer cell line MDA-MB-231. CHIP-exo assay was performed to identify genome-wide ATF4-binding sites after YW3-56 treatment, and 579

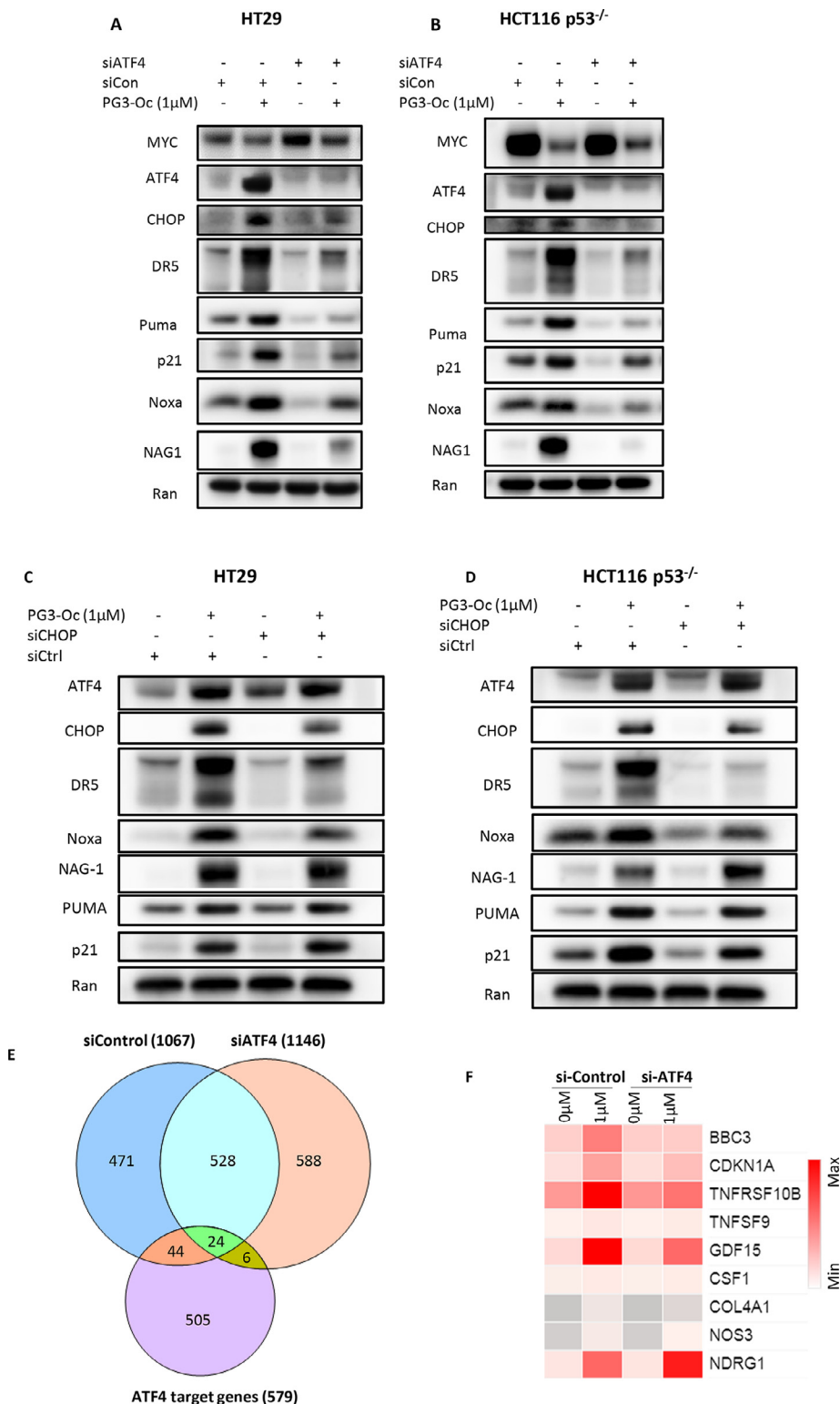


Fig. 5. ATF4 is a mediator of PG3-Oc-induced p53 pathway restoration. HT29 (A) and HCT116 p53^{-/-} (B) cells were transfected with Control and ATF4 siRNAs, and at 24hr after transfection, the cells were treated with 1 μM PG3-Oc for 24 h. Then cell lysates were prepared and western blot analysis were performed using indicated antibodies. HT29 (C) and HCT116 p53^{-/-} (D) cells were transfected with Control and CHOP siRNAs, and at 24 h after transfection, the cells were treated with 1 μM PG3-Oc for 24 h. Then cell lysates were prepared and western blot analysis were performed using indicated antibodies. (E) HT29 cells were transfected with Control and ATF4 siRNAs, and at 24 h after transfection, cells were treated with/without 1 μM PG3-Oc for 24 h in triplicate, and RNA samples were prepared. RNA-Seq, and IPA analysis were performed (see Materials and Methods for details). Venn diagram shows that PG3-Oc induces ATF4 target gene expression. (F) Heat map and bar charts. (G and H) Analysis of some key p53 genes expression associated in apoptosis. (I) Common genes between known ATF4 target gene database and known p53 target gene data bases (Fischer’s and Riley’s databases). (J) Venn diagram analysis showed unique and overlapped genes identified in PG3-Oc treated si-Control and si-ATF4 cell lines in comparison with known p53 gene data-base.

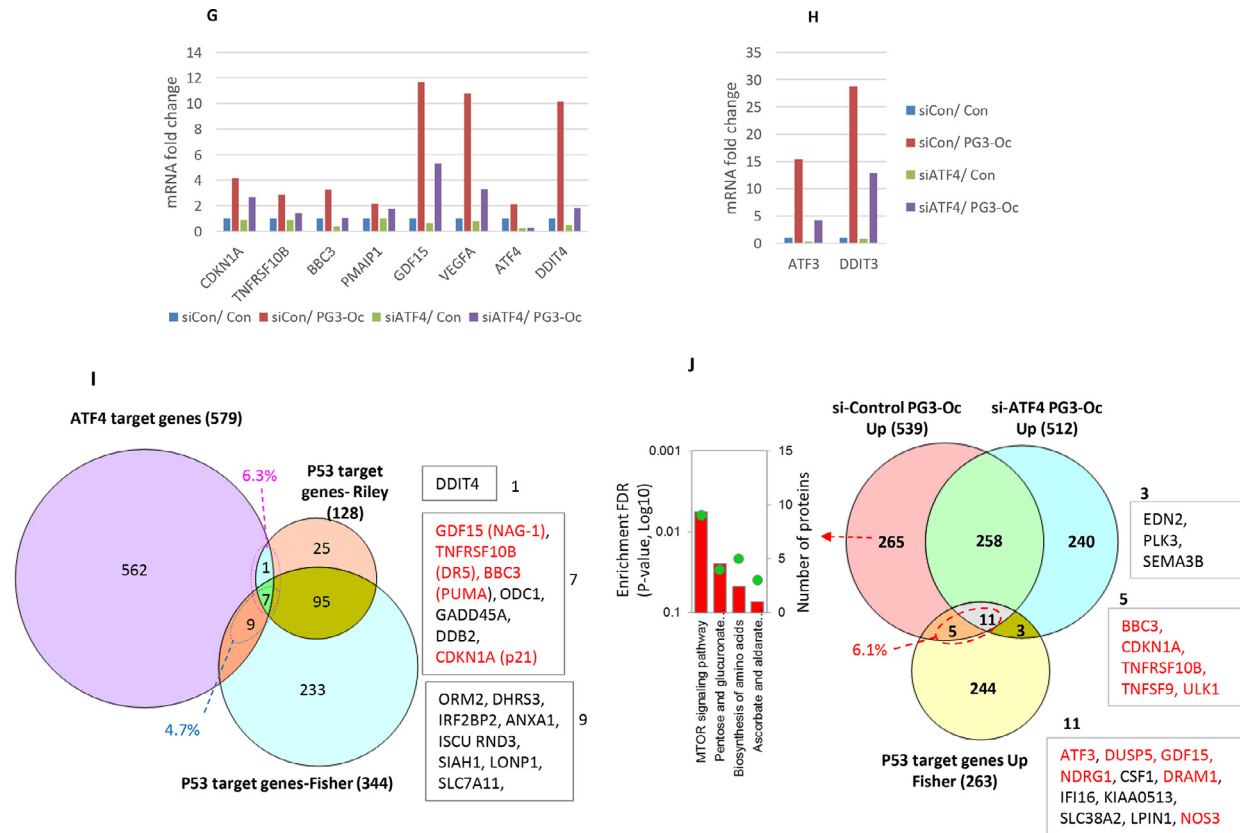


Fig. 5. Continued

possible ATF4 target genes were identified [20]. Using this ATF4 target gene data base, Venn diagram (Fig. 5E) was generated. 68 (44 + 24) ATF4 target genes are induced in control siRNA cells by PG3-Oc treatment. After knockdown of ATF4, the number decreased to 24 ATF4 target genes (Fig. 5E and Supplementary Table 7). Six new ATF4 target genes are induced after ATF4 knockdown, suggesting PG3-Oc also induces upregulation of ATF4 target genes in an ATF4-independent way (Fig. 5E). Among the 24 genes, RNA-seq data clearly show the mRNA levels of some genes are significantly decreased due to ATF4 knockdown (Fig. 5 F–H), such as GDF15 (NAG-1), VEGFA, CDKN1A (p21), DDIT4 (REDD-1), DDIT3 (CHOP), and ATF3. However, the fold changes of these genes remain higher than 2-fold, therefore IPA software still considers them as induced and includes them in the gene list. Based on these observations, the 6 genes are included as affected by ATF4 knockdown, so a total of 26 (20 + 6) genes are significantly downregulated, that is a total of 39.4% (26/66) of the ATF4 target genes induced by PG3-Oc are downregulated by ATF4 knockdown.

To find out the percentage of ATF4 target genes that are p53 target genes, a Venn diagram was generated using the ATF4 target gene base and 2 p53 target gene databases (Fig. 5I and Supplementary Table 8) [4,10,20]. 16 common genes between ATF4 and Fischer's p53 gene data are found, that is 4.7% (16/344). Eight common genes between ATF4 and Riley's p53 gene database are found, that is 6.3% (8/128). The common gene set (Fig. 5I box 7) contains important target genes that regulate cell apoptosis as indicated in red.

PG3-Oc induces upregulation of 16 p53 target genes, which is 6.1% (16/263) of the 263 p53 target genes (Fig. 5J). Among the 16 p53 target genes, after knockdown of ATF4, 5 genes are significantly downregulated (Fig. 5J box 5 and Supplementary Table 5). ATF3 and GDF15 (Fig. 5G and H) are also significantly downregulated, however their mRNA levels are still higher than 2-fold, therefore the 2 genes are shown in common block

11 (Fig. 5J) box 11). Based on these observations, a total of 7 (5 + 2) genes among the 16 genes are significantly downregulated after ATF4 knockdown, which indicates that 43.8% (7/16) p53 target genes induced by PG3-Oc are affected by knockdown of ATF4. A set of 265 genes is unique in siControl-PG3-Oc-treated HT29 cells, and KEGG gene enrichment analysis indicates mTOR signaling pathway and biosynthesis of amino acids are significantly affected, which is consistent with ATF4 activation (Figs 5J and S7 E).

In summary, ATF4 regulates expression of a sub-set of key p53 target genes, which are involved in the regulation of the cell cycle and apoptosis.

PG3-Oc-induced upregulation of ATF4 is not through canonical ER stress

ER stress or the integrated stress response (ISR) activate the UPR (unfolded protein response) signaling pathway. Canonical ER stress activates ATF4 through the PERK/eIF2 α /ATF4 pathway, and ISR activates ATF4 through the PKR (or GCN2 or HRI)/eIF2 α /ATF4 pathway. Both pathways result in upregulation of ATF4 protein at a post-transcriptional level. To determine which pathway mediates PG3-Oc-induced upregulation of ATF4, time-course studies were performed (Fig. 6A and B). Time-dependent induction of phosphorylation of Ser51 of eIF2 α , upregulation of ATF4, and its target genes CHOP and PUMA is observed in both HT29 and HCT116 p53^{-/-} cell lines (Fig. 6A and B). Another ER stress marker GRP78 is induced in a time-dependent way in HT29 cells, but not in HCT116 p53^{-/-} cells (Fig. 6A and B). Thapsigargin (TG) is a known ER stress inducer and used as a positive control. GSK2606414 is a selective and potent inhibitor of PERK. As shown in Fig. 6C, HT29 cells were treated for 5 h. The PERK inhibitor potently inhibits TG-induced phosphorylation of Ser51 of eIF2 α , upregulation of ATF4, and its target gene CHOP, but

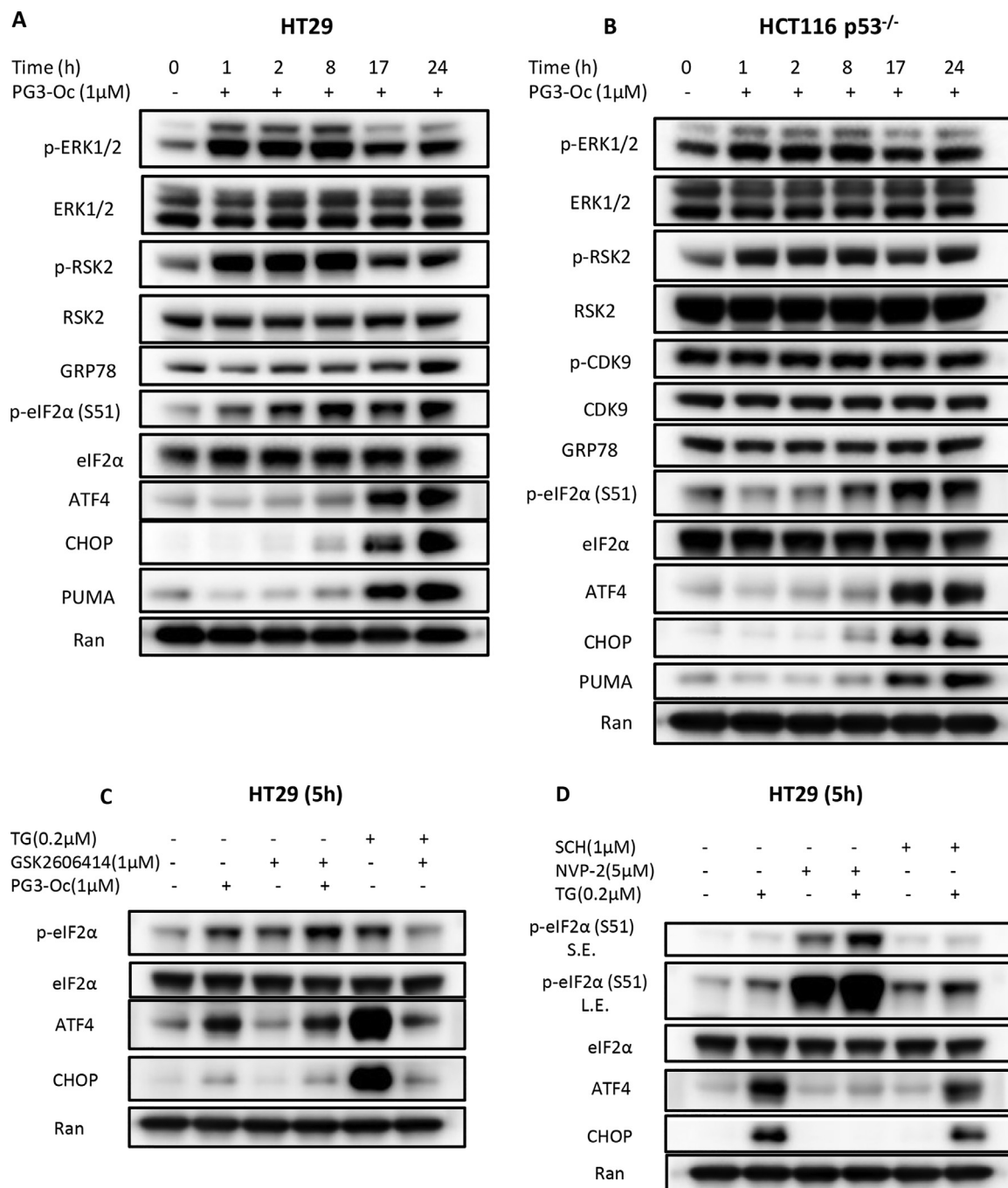


Fig. 6. PG3-Oc-induced upregulation of ATF4 is not through ER stress HT29 (A) and HCT116 p53^{-/-} (B) cells were treated with PG3-Oc at different time points as indicated in the Figure A and B. Cell lysate were prepared and western blots were performed using indicated antibodies. (C) HT29 cells were treated with GSK2606414, TG and PG3-Oc for 5 hr, and then cell lysates were prepared and western blots were performed using indicated antibodies. (D) HT29 cells were treated with thapsigargin (TG), SCH772984 (SCH) and NVP-2, respectively or combined treatments. Cell lysates were prepared and western blots were performed using indicated antibodies.

has no effect on PG3-Oc-induced phosphorylation of eIF2 α , upregulation of ATF4, and CHOP. These data clearly indicate that PG3-Oc-induced upregulation of ATF4 is not through canonical ER stress. This observation was further confirmed by 24 h treatment of HT29 cells (Fig. 7B). The PERK inhibitor does not attenuate PG3-Oc-induced upregulation of ATF4 protein and upregulation of ATF4 downstream gene expression of CHOP, PUMA, p21, NAG-1, DR5, and Noxa. In addition, the PERK inhibitor also does not block phosphorylation of ERK2, suggesting that PG3-Oc-induced

upregulation and activation of ATF4 is also not through noncanonical ER stress PERK/ERK2/ATF4 pathway as reported [18].

In addition, IPA canonical pathway analysis indicates that the UPR signaling pathway is one of the top hits (second place) in siControl and PG3-Oc treated cells; after ATF4 knockdown, the UPR pathway moved down to fourth place, suggesting suppression of UPR signaling (Fig. S7 A and B). Importantly, the color code for UPR signaling pathway is grey, indicating that the pathway has no activity identified by the analysis, which is

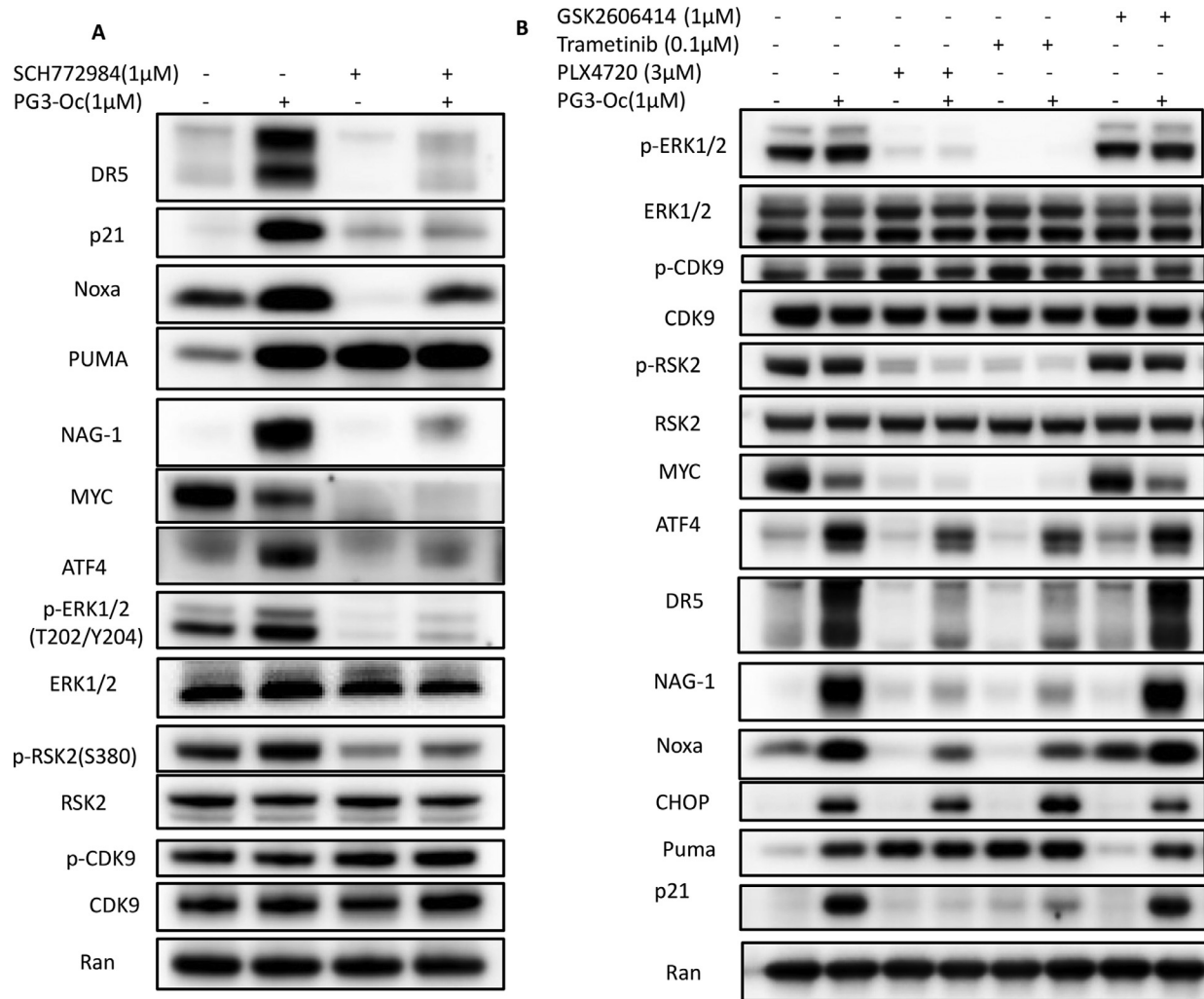


Fig. 7. ERK1/2 and CDK9 kinase functions are required for ATF4 transcriptional activity. (A) HT29 cells were treated with PG3-Oc or SCH772984 (SCH) respectively, or co-treatment with PG3-Oc/SCH772984 for 28 h. (B) HT29 cells were treated with PG3-Oc, trametinib (Tram), PLX4720 (PLX) and GSK2606414 respectively, or co-treatment with PG3-Oc/trametinib, PG3-Oc/PLX4720, and PG3-Oc/GSK2606414 for 24 h. (C) HCT116 p53^{-/-} were treated with PG3-Oc, SCH772984, trametinib, and PLX4720, respectively, or co-treatment with PG3-Oc/SCH772984, PG3-Oc/trametinib and PG3-Oc/PLX4720 overnight. (D) HT29 cells were treated with PG3-Oc, LDC 000067 (LDC), and NVP-2, respectively, or co-treatment with PG3-Oc/LDC000067 or PG3-Oc/NVP-2 overnight. HT29 (E) and HCT116 p53^{-/-} (F) cells were treated with PG3-Oc, or NVP-2 respectively, or co-treatment with PG3-Oc/NVP-2 overnight. (G) Proposed model of PG3-Oc-induced partial restoration of p53 pathway through ATF4 transcriptional modulation by ERK1/2 and CDK9.

consistent with our observation that ATF4 is not activated through ER stress. Therefore, PG3-Oc-induced upregulation of ATF4 is through an unknown non-canonical ER stress pathway.

ERK1/2 and CDK9 kinase functions are required for ATF4 transcriptional activity

Recent papers reported that phosphorylation of ATF4 by ERK2 or CDK9 stabilizes and promotes ATF4 nuclear translocation and ATF4 transcriptional function downstream of canonical ER stress [18,47]. Phosphorylation sites of ATF4 by ERK2 or CDK9 are different [18,47]. Our time-course experiments indicate that PG3-Oc treatment increases phosphorylation of ERK2 and its direct substrate RSK2 in both HT29 and HCT116 p53^{-/-} cell lines (Fig. 6A and B), indicating ERK2 kinase activation. PG3-Oc does not increase the basal level of phosphorylation of CDK9 kinase (Fig.s 6B, 7B and E), suggesting the compound has no effect on CDK9 kinase activity.

We investigated whether ERK2 or CDK9 regulate non-canonical ER stress-induced ATF4 transcriptional activity. To address this question, we used the highly specific and potent ERK1/2 inhibitor SCH772984 and the CDK9 inhibitor NVP-2. SCH772984 significantly and NVP-2 completely blocks thapsigargin-induced upregulation of ATF4 and its target gene CHOP without inhibition of phosphorylation of eIF2 α , demonstrating that ERK2 and CDK9 kinases function downstream of canonical ER stress (Fig. 6D). That is consistent with the results of the publications mentioned above.

The ERK2 inhibitor blocks PG3-Oc-induced upregulation of ATF4 and CHOP, DR5, p21, Noxa and NAG-1 in both HT29 and HCT116 p53^{-/-} cell lines (Fig. 7A and C), demonstrating ERK2 kinase activity is required for ATF4 stabilization and transcriptional function. As shown in Fig. 7A and C, the ERK1/2 inhibitor treatment alone results in potent downregulation of MYC and upregulation of PUMA, therefore, blockage of PG3-Oc-induced PUMA upregulation by SCH772984 is not observed.

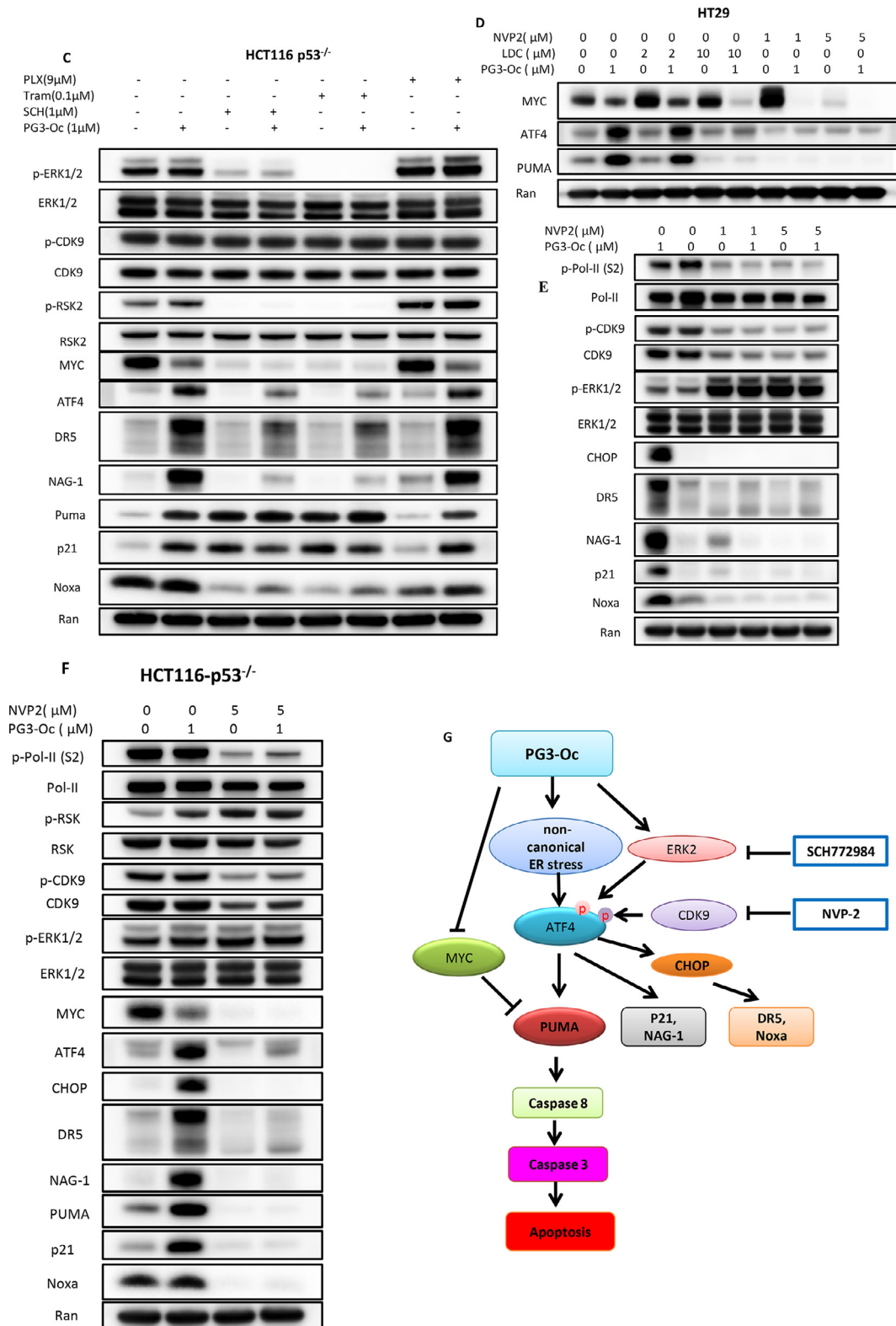


Fig. 7. Continued

The ERK2 inhibitor has no effect on phosphorylation of CDK9 in either HT29 or HCT116 p53^{-/-} cell lines (Fig. 7A and C), suggesting that CDK9 is not a substrate of ERK2. This is consistent with ERK2 phosphorylation sites of ATF4 being different from CDK9 phosphorylation sites of ATF4.

It is well-known that inhibition of MEK or Raf kinases leads to inhibition of ERK1/2 kinases. To further confirm these observations, HT29 and HCT116 p53^{-/-} cells were treated with MEK-specific inhibitor trametinib or mutant B-Raf (V600E)-specific inhibitor PLX4720 with or without PG3-

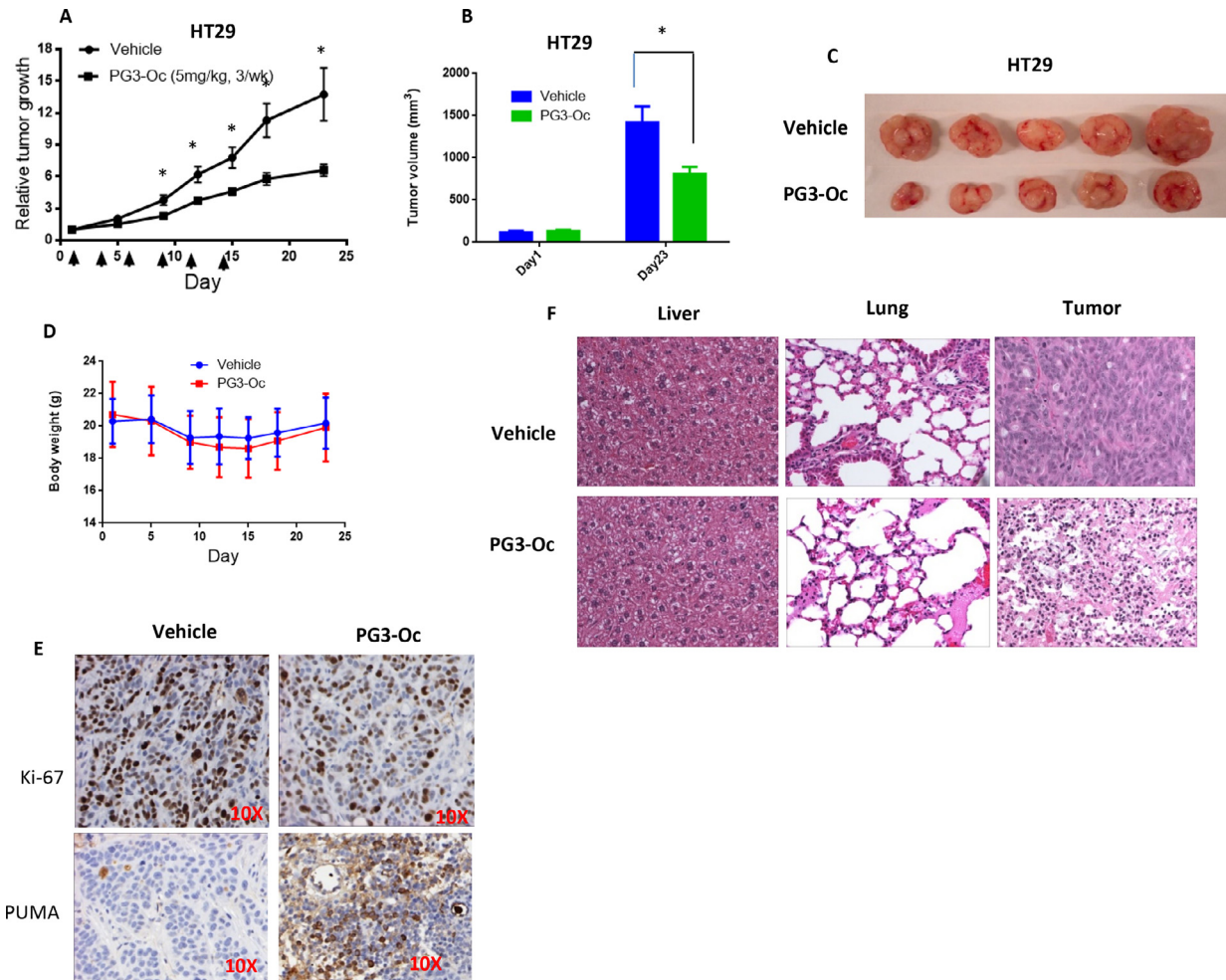


Fig. 8. Established HT29 xenografts were treated with 5 mg/kg PG3-Oc and vehicle control 3 times weekly for a total 6 treatments. The arrows show the days of the treatment. (A) The relative tumor growth is normalized tumor size to the tumor size of day 1 before the treatment ($*P < 0.05$ by an unpaired *t* test). (B) The mean tumor volume before and after treatment ($*P < 0.05$ by an unpaired *t* test). (C) Images of 5 representative tumors from vehicle control and treated groups. (D) Body weight changes of nude mice during treatment period ($*P < 0.05$ by an unpaired *t* test). Error bar correspond to SEM. (E) Ki-67 and PUMA antibody staining of HT29 tumors. (F) H&E staining of liver, lung and HT29 tumors.

Oc. The MEK inhibitor potently inhibits ERK1/2 kinases, indicated by potent inhibition of phosphorylation of both ERK1/2 and its substrate RSK2 in both HT29 and HCT116 p53^{-/-} cell lines (Fig. 7B and C). PLX4720 potently inhibits ERK1/2 kinases in HT29 cells, as both phosphorylation of ERK1/2 and RSK2 are potently inhibited (Fig. 7B), but not in HCT116 p53^{-/-} cells (Fig. 7C). The HT29 cell line harbors mutant B-Raf (V600E), and HCT116 p53^{-/-} cell line has wild-type B-Raf which is not inhibited by PLX4720. Trametinib or PLX4720 impede PG3-Oc-induced upregulation of ATF4 and DR5, p21, NAG-1, and Noxa in HT29 cells, respectively, thus phenocopying the effects of the ERK1/2 inhibitor. Trametinib also prevents PG3-Oc-induced upregulation of ATF4 and DR5, p21, NAG-1, and Noxa in HCT116 p53^{-/-} cells, which again phenocopies the effects of the ERK1/2 inhibitor. On the other hand, PLX4720 does not inhibit wild-type B-Raf in HCT116 p53^{-/-} cells as shown in Fig. 7C, where phosphorylation levels of both ERK1/2 and RSK2 are maintained as the untreated control, PG3-Oc induces upregulation of ATF4. DR5, p21, NAG-1, Noxa, and PUMA are not affected by PLX4720 treatment, which supports the idea that ERK2 kinase activity is required for ATF4 stabilization and transcriptional function. Also, trametinib or PLX4720 treatment alone leads to potent downregulation of MYC and upregulation of PUMA respectively, which phenocopies ERK1/2 inhibitor SCH772984 again (Fig. 7B and C).

HT29 cells were treated with CDK9 inhibitor NVP-2 or LDC000067. LDC000067 impedes the upregulation of ATF4 and PUMA at 10 μ M concentration. NVP-2 abolishes the induction of ATF4 and PUMA at both 1 μ M and 5 μ M concentrations. Interestingly, LDC000067 alone does not induce MYC downregulation at 10 μ M concentration, but enhances PG3-Oc-induced MYC degradation. By contrast, NVP-2 alone and cotreatment with PG3-Oc potently downregulates MYC protein level (Fig. 7D).

We noticed that PUMA was not upregulated though MYC was potently downregulated in HT29 (Fig. 7D) and HCT116 p53^{-/-} cells (Fig. 7F) because PG3-Oc-induced upregulation of ATF4 was abolished by the CDK9 inhibitor. These results support our model that both MYC degradation and ATF4 upregulation are required for PUMA induction by PG3-Oc.

Since NVP-2 is more potent and more specific than LDC000067, HT29 cell lysates treated with NVP-2 and NVP-2/PG3-Oc co-treatment from same experiment (Fig. 7D) were used for further western blot analysis shown in Fig. 7E.

HT29 (Fig. 7E) and HCT116 p53^{-/-} cells were treated with NVP-2 or cotreated with NVP-2/PG3-Oc (Fig. 7F). CDK9 directly phosphorylates Ser 2 of RNA polymerase II CTD (pol II) during elongation of the transcripts [47]. We observed that the phosphorylation of both CDK9 and RNA polymerase II CTD is potently inhibited by NVP-2 alone or combined

treatment. Interestingly, NVP-2 does not show any effects on PG3-Oc-induced phosphorylation of ERK1/2, suggesting that ERK1/2 are not a substrate of CDK9. Importantly, inhibition of CDK9 abolishes PG3-Oc-induced upregulation of ATF4 and DR5, NAG-1, PUMA, p21, Noxa, and CHOP.

In summary, inhibition of either ERK2 or CDK9 blocks PG3-Oc-induced upregulation and activation of ATF4. ERK2 and CDK9 together regulate ATF4 stability and transcriptional activities downstream of both thapsigargin-induced canonical and PG3-Oc-induced non-canonical ER stress. We propose a model of upregulation and activation of ATF4 by PG3-Oc and ATF4 mediates partial restoration of p53 pathway (Fig. 7G).

Lack of genotoxic stress by PG3-Oc

DNA damage induces the p53 pathway and leads to cell apoptosis. To study whether the p53 pathway restoration by compound PG3-Oc is due to DNA damage, we investigated the uptake and localization of PG3-Oc in cells. PG3-Oc and prodigiosin are red fluorescent compounds, and their localization in live cells can be monitored by fluorescence microscopy. We found that PG3-Oc and prodigiosin rapidly enter cells within 2 h of incubation and remain in the cytosol at the 8-h time point in HT29 and SW480 cells (Fig. S8 A). Since we already observed that 1 μ M PG3-Oc treatment for 8 h can prominently induce the upregulation of PUMA mRNA (Fig. 2A–C) in HT29, SW480, and HCT116 p53^{-/-} cells, we investigated the DNA damage marker γ -H2AX (phospho Ser 139-histone H2AX) expression after the treatment for 8 h. Western blot analysis shows that PG3-Oc and prodigiosin do not induce γ -H2AX in HT29 and SW480 cells at lower doses required for p53 pathway activation (Fig. S8 B). Immunofluorescence staining shows that 1 μ M PG3-Oc and prodigiosin does not induce γ -H2AX focus formation after the 8-h treatment. By comparison, the DNA damaging chemotherapeutic drug CPT-11 used as a positive control significantly induces γ -H2AX foci in HT29 and SW480 cells (Fig. S8 C). Both western blot and immunofluorescence staining data are consistent with the cytoplasmic localization of PG3-Oc. Our data indicate that the restoration of the p53 pathway by PG3-Oc at low concentrations does not show genotoxic effects in mutant p53-expressing cancer cells.

In vivo studies of PG3-Oc demonstrate anti-tumor efficacy

To evaluate the antitumor effects of PG3-Oc in vivo, we established human tumor xenograft models by subcutaneous injection of human colon cancer cells into nude mice. After the tumor volume reached approximately 50 mm³, with HT29 xenografts, mice were treated by i.p. injection with vehicle or PG3-Oc at 5 mg/kg³ times weekly for 2 wk. The tumor volume in PG3-Oc-treated mice is significantly reduced as compared with vehicle-treated mice (Fig. 8A–C). No significant difference in body weight is observed between PG3-Oc and the vehicle treatment groups (Fig. 8D). Ki-67 expression is significantly decreased in PG3-Oc-treated tumors as compared with the vehicle group (Fig. 8E). PUMA is significantly induced in PG3-Oc-treated tumors as compared with controls (Fig. 8E). No in vivo toxicity is observed as indicated by H&E staining of tissues (Fig. 8F). These results indicate that PG3-Oc inhibits tumor growth in the HT29 mouse xenograft model.

With HCT116 p53^{-/-} xenografts, mice were treated by i.p. injection with vehicle or PG3-Oc•HCl at 7.6 mg/kg/day for biomarker studies (Fig. S9 A–C). As shown in Fig. S9 G, Western blot indicates that PG3-Oc•HCl induces significant upregulation of ATF4, PUMA and apoptosis markers of cleaved caspase 3 and cleaved PARP. IHC (immunohistochemistry) staining indicates that PG3-Oc•HCl induces upregulation of ATF4, PUMA and cleaved caspase 3 and downregulation of Ki-67 in HCT116 p53^{-/-} xenografts (Fig. S9 B and C). However, tumor volume in treated mice appears to be not significantly different compared with vehicle-treated mice (Fig. S9 D and

E). On day 12, there was a reduction of in body weight. The treatment was stopped for 4 days, and then continued. No significant difference in body weight is observed between treated and the control groups (Fig. S9 F).

We note that the conditions of the in vivo studies are not optimized, and we plan to perform more experiments in the future, including further studies of pharmacokinetics and toxicity of PG3-Oc, at different doses and treatment schemes, etc.

Discussion

This is the first report on the compound PG3-Oc, a novel chemical entity (El-Deiry et al., 2017; issued composition of matter patent). Our manuscript describes therapy-induced p53-independent restoration of the p53 transcriptome. The prior literature typically investigated a few p53 targets and claimed p53 pathway restoration. It is necessary to evaluate the transcriptome and describe the extent of p53 pathway restoration by novel therapeutic candidates that act in a manner independent of p53. In this manuscript we have also evaluated the p53-independent p53 pathway-associated proteome by a novel p53 pathway restoring compound. There is little prior literature that has rigorously defined the p53-activated proteome following treatment by any drug and so we created an in-house p53-activated proteome data-base. An aspect of our approach that often gets misunderstood is the expectation that p53 pathway-restoring drugs act by altering mutant p53 protein and that such compounds have correlate activities in cells such as p53-specific genomic DNA-binding and chromatin association through mutant p53. This is not how the drugs that emerge from our functional p53-reporter screens work. Thus, this paper shows how a different transcription factor, ATF4 can “restore” p53 target gene-activation after drug treatment, essentially bypassing the defective mutated-p53 pathway. We evaluated the effect of the drug on the transcriptome and proteome. We show in vivo activity of the compound that is significant single-agent efficacy but this has not been optimized, and no maximally-tolerated dose (MTD) has been determined. This manuscript points to the ATF4 pathway with a specific therapeutic agent and claims partial (and significant) global p53-pathway restoration. The compound is also interesting because it targets Myc for degradation, an additional activity that we believe is relevant to its anti-tumor efficacy. Insights are included for non-canonical ER stress-independent activation of ATF4 by ERK1/2 and CDK9.

Restoration of the p53 pathway has been a long-term goal of the field of cancer research as an approach to treat tumors with mutated p53 and aggressive clinical behavior. The current work demonstrates the feasibility of the approach for small molecule drug-induced cellular reprogramming to achieve partial restoration of the global p53 transcriptome and proteome, in a p53-independent manner. Our dissection of the molecular components led us to identify ATF4 as a key transcription factor mediating the expression of p53 target genes in p53 mutant and null cancer cell lines after PG3-Oc treatment. Previously, ATF4 stabilization was thought to be regulated by ER stress (PERK-eIF2 α signaling) or IRS (GCN2/PKR/HRI-eIF2 α signaling), and phosphorylation of eIF2 α at serine 51 is required. Very recently, it was discovered that mitochondrial protease ClpP (caseinolytic protease P) activation by ONC201 results in ATF4 increase without increase in phosphorylated eIF2 α in Z138 cells [48]. In addition, regulation of ATF4 through other mechanisms was reported recently, such as phosphorylation of ATF4 by ERK2, RSK2 and CDK9 stabilizes ATF4 and promotes ATF4 translocation into the nucleus [18,47,49]. We show that ATF4 shares a subset of p53 target genes that are involved in cell cycle arrest and apoptosis. This suggests that ATF4 is a critical node for responding to various intrinsic and extrinsic stresses and regulating cell fate.

Rescue of deficient or lost p53 function is an attractive strategy for cancer therapy. p53-restoring compounds usually act on specific p53 mutations, such as R273H (APR-246) or R175H (ZMC1) [2]. Toxicity, off-target effects and limited activity have been roadblocks for these different small molecules

to progress to the clinic although progress is being made [2]. However, there is still a major unmet medical need to target tumors harboring mutant p53. Since thousands of mutations of p53 have been reported [50,51], these kinds of drugs targeting specific mutations may have a somewhat limited use in clinic. In this regard, functional restoration of the p53 pathway using small molecules regardless of what kind of p53 mutations exist in the tumor cells is an attractive method to target mutant p53-bearing tumors. PG3-Oc potently induces cancer cell death through ATF4-mediated restoration of p53 pathway in various mutant p53-expressing cancer cells, including single, double, multiple, truncated, frameshift mutations or p53-null cancer cells (Table 1, Figs 1–3). These results indicate the versatility of a candidate therapeutic such as PG3-Oc to restoring the p53 pathway in cancer cells carrying various p53 mutants.

We propose a model (Fig. 7G) in which activation of ATF4 through non-canonical ER stress by PG3-Oc results in upregulation of PUMA, DR5, p21, and NAG-1. Both ERK2 and CDK9 kinase activities are required for the stabilization and transcriptional activity of ATF4. We also identify that both MYC downregulation and ATF4 upregulation are required to induce upregulation of PUMA, and PUMA-mediated activation of caspase 8 causes cell apoptosis. It is clear that MYC downregulation occurs independently of ATF4 in PG3-Oc treated cells, as knockdown of ATF4 does not block MYC downregulation by PG3-Oc (Fig. 5A and B). It is noteworthy that PG3-Oc targets MYC for degradation and that may contribute to its anticancer effect. As monotherapy, PG3-Oc shows significant anti-tumor efficacy with lack of toxicity in our *in vivo* studies.

The activation of ATF4 as a drug-induced mechanism to partially restore the p53 pathway provides an understanding for how treatment of cancer cells by a small molecule can restore critical anti-tumor p53 signaling in cells with mutant p53 and without involvement of p53 family members such as p73 or p63. While largely nonoverlapping the ATF4 and p53 transcriptomes appear to overlap at a critical set of effector genes that confer antitumor properties such as apoptosis induced by PUMA. Moreover, while each transcription factor regulates a set of genes that mediate its cellular effects, there are some common themes even where the additional gene sets are non-overlapping.

A major effect of PG3-Oc is to activate ATF4 which plays an important role in communicating pro-survival and pro-apoptotic signals. ER stress, the integrated stress response and mitochondrial stress lead to activation of ATF4. As a transcriptional factor, ATF4 regulates a transcriptional program involved in upregulation of p21 for cell cycle arrest and senescence; PUMA, DR5 and Noxa for apoptosis; ATG5 and ATG7 for autophagy, which are similar with p53. On the other hand, ATF4 also positively regulates gene expression involved in antioxidant response to protect cell from ROS (oxidative stress), and ER-associated degradation (ERAD) pathway for degradation of abnormal proteins, and re-establishment of cellular homeostasis. ATF4 and MYC co-regulate 30 MYC-target genes involved in amino acid biosynthesis and protein synthesis. These are different from p53. Final outcome of ATF4 activation is dependent on the cell type, nature of stressors and duration of the stresses [18–21].

Future work can focus in more detail on comparisons of the global and gene-specific regulation between ATF4 and p53, for example through ChIP-seq and single cell analysis. It will be important to unravel whether the PG3-Oc antitumor drug effects are primarily due to the partial restoration of the p53-transcriptome and -proteome that includes critical effector genes such as PUMA or whether other genes within the ATF4-transcriptome contribute to the drug efficacy. The insights from our paper could provide the basis for novel drug screens that optimize further the anti-tumor properties of both transcription factors, or investigate anticancer cooperativity in tumors that retain wild-type p53.

In the future it would be of interest to investigate similarities and differences in the ATF4-activated transcriptomes and general transcriptomes and proteomes between small molecule compounds such as ONC201 and PG3-Oc as both upregulate ATF4 although through different upstream

pathways. ONC201 is not known as a p53-pathway restoring compound although it was discovered as a TRAIL inducing compound (TIC10) and later found to induce DR5 through ATF4 and an integrated stress response involving HRI and PKR [52,53]. Thus, as there is more focus on ATF4 as a therapeutic target in cancer it will be important to understand the downstream drug effects that it mediates through different upstream regulators, as well as ATF4-independent effects, e.g., MYC suppression in the case of PG3-Oc. It will also be of interest to determine whether PG3-Oc relies on mitochondrial mechanisms involving ClpX and ClpP for ATF4 activation [48].

Conclusions

In summary, our results demonstrate that a small molecule can stimulate global p53 pathway restoration in tumor cells with mutated p53 or cells that are null for p53. This occurs in a p53 family-independent manner by PG3-Oc which impacts on a relevant transcriptome and proteome leading to tumor cell death. The mechanism of p53 pathway restoration by PG3-Oc involves activation of ATF4, which has a largely non-overlapping transcriptome with p53, but nonetheless activates critical targets required for drug-induced tumor suppression, including PUMA. The involvement of ATF4 in a partial global p53 pathway restoration represents a novel mechanism for therapy-induced molecular reprogramming to achieve an anti-cancer effect that may be translatable to the clinic.

Author Contributions

X.T., and W.S.E.-D. conceptualized the project and all experiments that were performed. X.T. was involved with the technical performance of all experiments. X.T., and W.S.E.-D. were involved in all of the data analysis and discussion of the results. N.A. performed proteomic experiments and analyzed proteomic dataset. S.Z. assisted with early compound testing. A. Lulla assisted with some Q-RT-PCR experiments and *in vivo* studies. A. Lev assisted with animal experiments. P.A. assisted with the CRISPR cloning strategy and experiments. D.T.D. assisted with flow cytometry. All authors were involved in writing and editing of the manuscript. W.S.E.-D. was responsible for administrative oversight of the research, securing funding for the project, and overall conduct of the experiments.

Supplementary Materials

There are 9 supplementary Figures with Legends included. In addition, there are an additional 22 source files available as spreadsheets/excel files that are relevant to the bioinformatic analyses.

Disclosure of Potential Conflict of Interest

W.S.E.-D. is a Founder of p53-Therapeutics, Inc., a biotech company focused on developing small molecule anti-cancer therapies targeting mutant p53. Dr. El-Deiry has disclosed his relationship with p53-Therapeutics and potential conflict of interest to his academic institution/employer and is fully compliant with institutional policy that is managing this potential conflict of interest.

Grant Support

The work was supported, in part, by the ACS and NIH grant CA176289 to W.S.E.-D.

Acknowledgments

The authors thank the Fox Chase Cancer Center genomics, Flow cytometry cores and bioinformatics facility for help with cell cycle analysis, real-time PCR experiments and RNA-Seq data analysis. This work has been presented in part at the 2017, 2018, and 2020 AACR meetings. W.S.E.-D. is an American Cancer Society Research Professor and is supported by the Menco Family Professorship at Brown University.

Supplementary materials

Supplementary material associated with this article can be found, in the online version, at doi:10.1016/j.neo.2021.01.004.

References

- [1] Vousden KH, Prives C. Blinded by the Light: The Growing Complexity of p53. *Cell* 2009;**137**:413–31.
- [2] Bykov VJN, Eriksson SE, Bianchi J, Wiman KG. Targeting mutant p53 for efficient cancer therapy. *Nat Rev Cancer* 2018;**18**:89–102.
- [3] Lin WC, Chuang YC, Chang YS, Lai MD, Teng YN, Su IJ, Wang CC, Lee KH, Hung JH. Endoplasmic reticulum stress stimulates p53 expression through NF-kappaB activation. *PLoS One* 2012;**7**:e39120.
- [4] Riley T, Sontag E, Chen P, Levine A. Transcriptional control of human p53-regulated genes. *Nat Rev Mol Cell Biol* 2008;**9**:402–12.
- [5] Andrysk Z, Galbraith MD, Guarnieri AL, Zaccara S, Sullivan KD, Pandey A, MacBeth M, Inga A, Espinosa JM. Identification of a core TP53 transcriptional program with highly distributed tumor suppressive activity. *Genome Res* 2017;**27**:1645–57.
- [6] Fei P, Bernhard EJ, El-Deiry WS. Tissue-specific induction of p53 targets in vivo. *Cancer Res* 2002;**62**:7316–27.
- [7] Allen MA, Andrysk Z, Dengler VL, Mellert HS, Guarnieri A, Freeman JA, Sullivan KD, Galbraith MD, Luo X, Kraus WL, et al. Global analysis of p53-regulated transcription identifies its direct targets and unexpected regulatory mechanisms. *Elife* 2014;**3**:e02200.
- [8] Kenzelmann Broz D, Spano Mello S, Biegging KT, Jiang D, Dusek RL, Brady CA, Sidow A, Attardi LD. Global genomic profiling reveals an extensive p53-regulated autophagy program contributing to key p53 responses. *Genes Dev* 2013;**27**:1016–31.
- [9] Menendez D, Nguyen TA, Freudenberg JM, Mathew VJ, Anderson CW, Jothi R, Resnick MA. Diverse stresses dramatically alter genome-wide p53 binding and transactivation landscape in human cancer cells. *Nucleic Acids Res* 2013;**41**:7286–301.
- [10] Fischer M. Census and evaluation of p53 target genes. *Oncogene* 2017;**36**:3943–56.
- [11] Mantovani F, Collavin L, Del Sal G. Mutant p53 as a guardian of the cancer cell. *Cell Death Differ* 2019;**26**:199–212.
- [12] Zhu J, Sammons MA, Donahue G, Dou Z, Vedadi M, Getlik M, Baryte-Lovejoy D, Al-awar R, Katona BW, Shilatifard A, et al. Gain-of-function p53 mutants co-opt chromatin pathways to drive cancer growth. *Nature* 2015;**525**:206–11.
- [13] Yu X, Vazquez A, Levine AJ, Carpizo DR. Allele-specific p53 mutant reactivation. *Cancer Cell* 2012;**21**:614–25.
- [14] Alexandrova EM, Yallowitz AR, Li D, Xu S, Schulz R, Proia DA, Lozano G, Dobbstein M, Moll UM. Improving survival by exploiting tumour dependence on stabilized mutant p53 for treatment. *Nature* 2015;**523**:352–356.
- [15] Zhang S, Zhou L, Hong B, van den Heuvel AP, Prabhu VV, Warfel NA, Kline CL, Dicker DT, Kopelovich L, El-Deiry WS. Small-Molecule NSC59984 Restores p53 Pathway Signaling and Antitumor Effects against Colorectal Cancer via p73 Activation and Degradation of Mutant p53. *Cancer Res* 2015;**75**:3842–52.
- [16] Chowdhury P, Lin GE, Liu K, Song Y, Lin FT, Lin WC. Targeting TopBP1 at a convergent point of multiple oncogenic pathways for cancer therapy. *Nat Commun* 2014;**5**:5476.
- [17] Hong B, Prabhu VV, Zhang S, van den Heuvel AP, Dicker DT, Kopelovich L, El-Deiry WS. Prodigiosin rescues deficient p53 signaling and antitumor effects via upregulating p73 and disrupting its interaction with mutant p53. *Cancer Res* 2014;**74**:1153–65.
- [18] Ojha R, Leli NM, Onorati A, Piao S, Verginadis II, Tameire F, Rebecca VW, Chude CI, Murugan S, Fennelly C, et al. ER Translocation of the MAPK Pathway Drives Therapy Resistance in BRAF-Mutant Melanoma. *Cancer Discov* 2019;**9**:396–415.
- [19] Tameire F, Verginadis II, Leli NM, Polte C, Conn CS, Ojha R, Salas Salinas C, Chinga F, Monroy AM, Fu W, et al. ATF4 couples MYC-dependent translational activity to bioenergetic demands during tumour progression. *Nat Cell Biol* 2019;**21**:889–99.
- [20] Wang S, Chen XA, Hu J, Jiang JK, Li Y, Chan-Salis KY, Gu Y, Chen G, Thomas C, Pugh BF, et al. ATF4 Gene Network Mediates Cellular Response to the Anticancer PAD Inhibitor YW3-56 in Triple-Negative Breast Cancer Cells. *Mol Cancer Ther* 2015;**14**:877–88.
- [21] Wortel IMN, van der Meer LT, Kilberg MS, van Leeuwen FN. Surviving Stress: Modulation of ATF4-Mediated Stress Responses in Normal and Malignant Cells. *Trends Endocrinol Metab* 2017;**28**:794–806.
- [22] Darshan N, Manonmani HK. Prodigiosin and its potential applications. *J Food Sci Technol* 2015;**52**:5393–407.
- [23] Prabhu VV, Hong B, Allen JE, Zhang S, Lulla AR, Dicker DT, El-Deiry WS. Small-Molecule Prodigiosin Restores p53 Tumor Suppressor Activity in Chemoresistant Colorectal Cancer Stem Cells via c-Jun-Mediated DeltaNp73 Inhibition and p73 Activation. *Cancer Res* 2016;**76**:1989–99.
- [24] El-Deiry WS, Tian X, Zhang S. Prodigiosin analogs. Patent, <https://patents.google.com/patent/US10654801B2>.
- [25] Franken NA, Rodermond HM, Stap J, Haveman J, van Bree C. Clonogenic assay of cells in vitro. *Nat Protoc* 2006;**1**:2315–19.
- [26] Ricci MS, Jin Z, Dews M, Yu D, Thomas-Tikhonenko A, Dicker DT, El-Deiry WS. Direct repression of FLIP expression by c-myc is a major determinant of TRAIL sensitivity. *Mol Cell Biol* 2004;**24**:8541–55.
- [27] Ahsan N, Belmont J, Chen Z, Clifton JG, Salomon AR. Highly reproducible improved label-free quantitative analysis of cellular phosphoproteome by optimization of LC-MS/MS gradient and analytical column construction. *J Proteomics* 2017;**165**:69–74.
- [28] Lomonosova E, Chinnadurai G. BH3-only proteins in apoptosis and beyond: an overview. *Oncogene* 2008;**27**(Suppl 1):S2–S19.
- [29] Carneiro BA, El-Deiry WS. Targeting apoptosis in cancer therapy. *Nat Rev Clin Oncol* 2020;**17**:395–417.
- [30] LeBlanc HN, Ashkenazi A. Apo2L/TRAIL and its death and decoy receptors. *Cell Death Differ* 2003;**10**:66–75.
- [31] Fernandez PC, Frank SR, Wang L, Schroeder M, Liu S, Greene J, Cocito A, Amati B. Genomic targets of the human c-Myc protein. *Genes Dev* 2003;**17**:1115–29.
- [32] Amente S, Zhang J, Lavadera ML, Lania L, Avvedimento EV, Majello B. Myc and PI3K/AKT signaling cooperatively repress FOXO3a-dependent PUMA and GADD45a gene expression. *Nucleic Acids Res* 2011;**39**:9498–507.
- [33] Yun S, Vincelette ND, Knorr KL, Almada LL, Schneider PA, Peterson KL, Flatten KS, Dai H, Pratz KW, Hess AD, et al. 4EBP1/c-MYC/PUMA and NF-kappaB/EGR1/BIM pathways underlie cytotoxicity of mTOR dual inhibitors in malignant lymphoid cells. *Blood* 2016;**127**:2711–22.
- [34] Smeenk L, van Heeringen SJ, Koeppl M, van Driel MA, Bartels SJ, Akkers RC, Denissov S, Stunnenberg HG, Lohrum M. Characterization of genome-wide p53-binding sites upon stress response. *Nucleic Acids Res* 2008;**36**:3639–54.
- [35] Melino G, Bernassola F, Ranalli M, Yee K, Zong WX, Corazzari M, Knight RA, Green DR, Thompson C, Vousden KH. p73 Induces apoptosis via PUMA transactivation and Bax mitochondrial translocation. *J Biol Chem* 2004;**279**:8076–83.

- [36] Pyati UJ, Gjini E, Carbonneau S, Lee JS, Guo F, Jette CA, Kellsell DP, Look AT. p63 mediates an apoptotic response to pharmacological and disease-related ER stress in the developing epidermis. *Dev Cell* 2011;**21**:492–505.
- [37] Chen D, Wei L, Yu J, Zhang L. Regorafenib inhibits colorectal tumor growth through PUMA-mediated apoptosis. *Clin Cancer Res* 2014;**20**:3472–84.
- [38] Dudgeon C, Peng R, Wang P, Sebastiani A, Yu J, Zhang L. Inhibiting oncogenic signaling by sorafenib activates PUMA via GSK3beta and NF-kappaB to suppress tumor cell growth. *Oncogene* 2012;**31**:4848–58.
- [39] Dudgeon C, Wang P, Sun X, Peng R, Sun Q, Yu J, Zhang L. PUMA induction by FoxO3a mediates the anticancer activities of the broad-range kinase inhibitor UCN-01. *Mol Cancer Ther* 2010;**9**:2893–902.
- [40] Ghosh AP, Klocke BJ, Ballestas ME, Roth KA. CHOP potentially co-operates with FOXO3a in neuronal cells to regulate PUMA and BIM expression in response to ER stress. *PLoS One* 2012;**7**:e39586.
- [41] Qing G, Li B, Vu A, Skuli N, Walton ZE, Liu X, Mayes PA, Wise DR, Thompson CB, Maris JM, et al. ATF4 regulates MYC-mediated neuroblastoma cell death upon glutamine deprivation. *Cancer Cell* 2012;**22**:631–44.
- [42] Zhao Z, Wang J, Tang J, Liu X, Zhong Q, Wang F, Hu W, Yuan Z, Nie C, Wei Y. JNK- and Akt-mediated Puma expression in the apoptosis of cisplatin-resistant ovarian cancer cells. *Biochem J* 2012;**444**:291–301.
- [43] Gao J, Senthil M, Ren B, Yan J, Xing Q, Yu J, Zhang L, Yim JH. IRF-1 transcriptionally upregulates PUMA, which mediates the mitochondrial apoptotic pathway in IRF-1-induced apoptosis in cancer cells. *Cell Death Differ* 2010;**17**:699–709.
- [44] Inoue Y, Kawachi S, Ohkubo T, Nagasaka M, Ito S, Fukaura K, Itoh Y, Ohoka N, Morishita D, Hayashi H. The CDK inhibitor p21 is a novel target gene of ATF4 and contributes to cell survival under ER stress. *FEBS Lett* 2017;**591**:3682–91.
- [45] Hu H, Tian M, Ding C, Yu S. The C/EBP Homologous Protein (CHOP) Transcription Factor Functions in Endoplasmic Reticulum Stress-Induced Apoptosis and Microbial Infection. *Front Immunol* 2018;**9**:3083.
- [46] Teske BF, Fusakio ME, Zhou D, Shan J, McClintick JN, Kilberg MS, Wek RC. CHOP induces activating transcription factor 5 (ATF5) to trigger apoptosis in response to perturbations in protein homeostasis. *Mol Biol Cell* 2013;**24**:2477–90.
- [47] Shiozaki Y, Okamura K, Kohno S, Keenan AL, Williams K, Zhao X, Chick WS, Miyazaki-Anzai S, Miyazaki M. The CDK9-cyclin T1 complex mediates saturated fatty acid-induced vascular calcification by inducing expression of the transcription factor CHOP. *J Biol Chem* 2018;**293**:17008–20.
- [48] Ishizawa J, Zarabi SF, Davis RE, Halgas O, Nii T, Jitkova Y, Zhao R, St-Germain J, Heese LE, Egan G, et al. Mitochondrial ClpP-Mediated Proteolysis Induces Selective Cancer Cell Lethality. *Cancer Cell* 2019;**35**:721–737 e9.
- [49] Oh YT, Liu X, Yue P, Kang S, Chen J, Taunton J, Khuri FR, Sun SY. ERK/ribosomal S6 kinase (RSK) signaling positively regulates death receptor 5 expression through co-activation of CHOP and Elk1. *J Biol Chem* 2010;**285**:41310–19.
- [50] Olivier M, Hollstein M, Hainaut P. TP53 mutations in human cancers: origins, consequences, and clinical use. *Cold Spring Harb Perspect Biol* 2010;**2**:a001008.
- [51] Freed-Pastor WA, Prives C. Mutant p53: one name, many proteins. *Genes Dev* 2012;**26**:1268–86.
- [52] Allen JE, Krigsfeld G, Mayes PA, Patel L, Dicker DT, Patel AS, Dolloff NG, Messaris E, Scata KA, Wang W, et al. Dual inactivation of Akt and ERK by TIC10 signals Foxo3a nuclear translocation, TRAIL gene induction, and potent antitumor effects. *Sci Transl Med* 2013;**5**:171ra17.
- [53] Kline CL, Van den Heuvel AP, Allen JE, Prabhu VV, Dicker DT, El-Deiry WS. ONC201 kills solid tumor cells by triggering an integrated stress response dependent on ATF4 activation by specific eIF2alpha kinases. *Sci Signal* 2016;**9**:ra18.